Pantanal Basin river muds from source to sink: compositional changes in a tropical back-bulge depozone

Edward L. Lo[1], Michael M. McGlue[1], Christopher J. Matocha[2], Aguinaldo Silva[3], Giliane G. Rasbold[1], Sidney Kuerten[4], Rômullo O. Louzada[5], and Kevin C. Haller[1]

[1]Department of Earth & Environmental Sciences, University of Kentucky, Lexington, KY, USA
[2]Department of Plant & Soil Sciences, University of Kentucky, Lexington, KY, USA
[3]Câmpus do Pantanal, Universidade Federal de Mato Grosso do Sul, Corumbá, Brazil
[4]Unidade Universitária de Campo Grande, Universidade Estadual de Mato Grosso do Sul, Campo Grande, Brazil
[5]Cidade Universitária, Universidade Federal de Mato Grosso do Sul, Campo Grande, Brazil

Author note:

Edward L. Lo https://orcid.org/0000-0003-3299-4495
Michael M. McGlue https://orcid.org/0000-0002-0725-7250
Christopher J. Matocha https://orcid.org/0000-0002-5574-7799
Aguinaldo Silva https://orcid.org/0000-0002-0630-9768
Giliane G. Rasbold https://orcid.org/0000-0001-7375-6261
Sidney Kuerten https://orcid.org/0000-0002-1714-0929
Rômullo O. Louzada https://orcid.org/0000-0002-7076-5282

Correspondence concerning this article should be addressed to Edward L. Lo, Georgia Southern University, 1100B Herty Bldg., 68 Georgia Ave., Statesboro, GA 30458. Email: elo@georgiasouthern.edu

Short title: Modern fluvial muds in the Pantanal Basin

Abstract
The Pantanal Basin is a low-gradient back-bulge analog for distal depozones associated with retroarc foreland basin systems in the geological record. Extensive lowland environments including fluvial megafans, floodplains, wetlands, and lakes make up the Pantanal Basin today, with detrital sediment sources located along basin-margin plateaus and remnants of ancient orogenic belts. Here, we examine the chemical composition and mineralogy of modern fine-fraction fluvial sediments using X-ray methods to assess the influence of chemical weathering on sediment composition in this tropical basin. The abundance of clay minerals follows the rank order pattern of kaolinite > vermiculite > illite > smectite. Kaolinite is more abundant in river muds from the north-central than the southern Pantanal, suggesting strong extant chemical weathering plus the potential for clays inherited from siliciclastic parent lithologies that formed under Mesozoic greenhouse conditions. Illite occurs in sediments draining the North Paraguay Belt and limited parts of the South Paraguay Belt, and it reflects the influence of mechanical weathering of the metamorphic facies. In the southeastern Pantanal, vermiculite is a dominant constituent of the Miranda River watershed, which drains dacitic parent rocks and rhodic ferralsols. The geochemistry of the sediments reveals the interplay of quartz addition and clays inherited from the parent rocks. The most quartzose sediments are encountered at the

confluence of the Paraguay River and the Taquari River megafan, where the cumulative effect of the 2 – 3-month flood pulse maximizes chemical weathering. Clay plus silt in back-bulge basins are controlled by climate > soils > parent rocks.

Lay summary

The compositional controls on clays and silts in tropical rivers of the Pantanal Basin distant from the Andes remain unclear. We collected 74 modern riverbank samples and used X-ray techniques to determine clay mineralogy and chemical elemental composition. The most common clay minerals in rank order of abundance were kaolinite > vermiculite > illite > smectite. Kaolinite was dominant in the north-central Pantanal, whereas vermiculite was dominant in the southeastern Pantanal. The most quartzose clays and silts were found in the middle Paraguay River Pantanal clays are controlled first by climate, and secondarily by soils.

Resumo

A Bacia do Pantanal é um sistema sedimentar de baixo relevo na região de *back-bulge* análoga no registro geológico a outros ambientes deposicionais associados com sistemas de retroarco. A hidrografia da Bacia do Pantanal inclui mega leques fluviais, planície de inundação, áreas alagadiças e lagos, com fontes de detritos provenientes das margens do planalto e resquícios de cinturões orogênicos pré-Cambrianos. Neste estudo, analisou-se a composição química e a mineralogia da fração fina de sedimentos fluviais modernos com métodos de raios-X para avaliar a influência do intemperismo químico na composição dos sedimentos nesta bacia tropical. A abundância de minerais de argila segue o padrão de ordem de caulinita > vermiculita > ilita > esmectita. A caulinita é mais abundante nos sedimentos fluviais do centro-norte do que no sul do Pantanal, o que sugere forte intemperismo químico recente além do potencial de argilas herdadas de fontes sedimentares siliclásticas formadas em condições de “greenhouse” durante a Era Mesozoica. A ilita ocorre em sedimentos que drenam a Faixa Norte do Paraguai e partes limitadas na Faixa Sul do Paraguai, refletindo a influência do intemperismo mecânico das fácies metassedimentares. No sudeste do Pantanal, a vermiculita é um constituinte dominante da bacia do Rio Miranda, que drena rochas-fonte dacíticas e latossolos vermelhos. A geoquímica dos sedimentos revela a interação entre a adiação de quartzo e as argilas herdadas das rochas-fonte. Os sedimentos quartzosos são mais frequentes na confluência do Rio Paraguai com o mega leque do Taquari onde o efeito cumulativo do pulso de inundação (2 a 3 meses) maximiza o intemperismo químico. Este estudo revela que a argila e o silte que preenchem bacias de *back-bulge* são controlados pelo clima > solos > rochas-fonte.

Keywords: Clay mineralogy, Geochemistry, Chemical weathering, Tropical wetlands

1. Introduction

Modern sands, silts and clays in large watersheds have been studied to reveal the interactions among parent lithology, climate, and tectonics that influence sediment composition (Johnsson, 1993; Jonell et al., 2017; He et al., 2020; Garzanti et al., 2021). For instance, quartz enrichment and kaolinite abundance in lowland settings or intense mechanical weathering on hillslopes are often linked to hot, humid conditions characteristic of the tropics (Oliva et al., 1999; Viers et al., 2000; Aristizábal et al., 2005; Garzanti et al., 2019). Tardy et al. (1973) show that montmorillinite can also be concentrated in the lowlands downstream of granites in humid tropical environments. These diverse floodplain clay mineral compositions suggest that considerable variability surrounds clay mineral development in tropical floodplains. Although studies on clay minerals have been conducted worldwide (e.g., Chamley, 1989), the relationships among fluvial transport, climate, tectonics, and chemical weathering on clay mineralogy are site-specific and require localized sediment sampling. Modern fluvial sediment compositions have not been systematically assessed in many South America rivers, with limited research focused on the composition of the suspended sediment load in a few major rivers (Potter, 1994; Guyot et al., 2007; McGlue et al., 2016; Repasch et al., 2020).

Climate gradients are essential controls on the weathering of clay minerals and impact regional vegetation and agricultural production. When hydrolysis is inefficient or incomplete, feldspar minerals persist along with Ca^{2+} and Na^{+}, as was observed along the Zambezi River system (Garzanti et al., 2022). No clay minerals may be observed in exceptionally arid conditions (e.g., Warr et al., 2022). Where the climate is warm and humid, the 1:1 type clays are predominant with greater kaolinite compared to illite/mica in the clay (<2 μm) fraction (Ito & Wagai, 2017). These large-scale trends have been documented and used for understanding the chemical weathering processes globally. Changes to the clay mineral assemblage and fine fraction geochemistry along the Pearl River and the Red River were dominantly controlled by climate gradients (He et al., 2020, 2022). However, none of these have examined modern fluvial clays within a primarily floodplain or wetland environment. Garzanti et al. (2011) provided the most comprehensive study of floodplain clays on the Indian sub-continent, within the Ganges-Brahmaputra foreland basin system.

Parent lithology is a secondary determinant of modern clay minerals. Guyot et al. (2007) examined clay minerals across the Amazon Basin and found that the provenance of the areas (shield, Andean cordillera, Piedmont basins) determined the clay mineral constituents. For example, the illite and chlorite reflected erosion of the metapelites and metabasites exposed in the Red River basin (He et al., 2022). Kaolinite can originate from virtually any parent rock, given warm and humid environments typical of the tropics (Dill, 2016). Tropical and sub-tropical climates commonly result in an under-representation of mafic lithologies relative to their areal extent in modern fluvial sediments (Garzanti et al., 2014; Hatzenbühler et al., 2022).

Mud composition can reflect differences between transport-limited erosion and weathering-limited erosion depending on the land surface gradient and hydrology (Stallard et al., 1991). Sediment erosion can be considered transport-limited, where weathering creates more clays than can be transported, resulting in profoundly weathered soil profiles (Stallard et al., 1991). Plateaus and floodplains are emblematic of transport-limited erosional regimes where the sediments and soils remain in place, subjected to prolonged chemical weathering. Weathering-limited erosion occurs when the bedrock is partially weathered before the sediment is removed, concentrating micas and feldspars (Stallard et al., 1991). Cordilleras erode physically through rockfalls and the breakdown of the rock formation, exacerbated by high slopes. Further understanding of these and other source-to-sink processes requires a close examination of weathering intensity, as recorded in clay mineral composition and elemental geochemistry (He et al., 2020; Cruz et al., 2022).

Back-bulge basins are an ideal locale to examine how changes in environmental conditions affect clay mineral production in tropical riverine settings. Back-bulges are usually low-gradient zones that store sediment and preserve important environmental signals over geologic time (Horton & DeCelles, 1997; Assine et al., 2016; Brewer et al., 2020; Caracciolo, 2020). Silt plus clay preservation is excellent in low-gradient back-bulge depositional environments (e.g., in floodplains, lakes, and wetlands) (Quartero et al., 2015; McGlue et al., 2016; Tineo et al., 2022). Therefore, one of the motivations of this research is to examine the processes that control mud mineralogy and chemistry in a modern tropical setting where the environmental gradients (i.e., climate, soils, vegetation, relief) are relatively well-understood in order to provide insights that may improve interpretations of the geological record. We selected the Pantanal Basin as an exceptional locale to examine the primary sedimentary processes. The Pantanal Basin (Brazil/Bolivia/Paraguay) forms the back-bulge depozone of the Cenozoic Andean foreland basin (Chase et al., 2009; Cohen et al., 2015; Horton, 2022). The Pantanal is a tropical savanna extending from the Amazon drainage divide to the Brazilian border with Paraguay (Figure 1A) (Beck et al., 2018). Most hinterland (i.e., basin margin) lithologies surrounding the Pantanal are siliciclastic sedimentary rocks, with some pre-Cambrian igneous and metamorphic exposures; these lithologies were recently grouped into six provenance regions (Figure 1B, C; Lo et al., 2023).

In this study, modern mud in the rivers of the Pantanal were collected to evaluate their mineralogy and chemical composition. We employed X-ray diffraction (XRD) for semi-quantitative clay mineralogy and wavelength-dispersive X-ray fluorescence (WD-XRF) to deduce major elemental geochemistry (Moore & Reynolds, 1989). These data were analyzed along with environmental characteristics of the basin's sub-watersheds (e.g., slope, lithology, precipitation, elevation) to elucidate the processes that control clay composition. We tested the hypothesis that differences in mean annual precipitation control the clay mineral assemblage in modern fluvial silt plus clay in the Pantanal. This article is a companion study to a petrographic analysis of contemporary river sands in the Pantanal (Lo et al., 2023), with the end goal of identifying major patterns in sediment generation and transport in this basin. Plata River samples were integrated with this study to evaluate the influence of Pantanal Basin clay composition on downstream sediments. Ultimately, our objective is to improve interpretations of ancient sedimentary rocks in similar settings through a detailed set of modern observations and a database of mineralogical and chemical measurements.

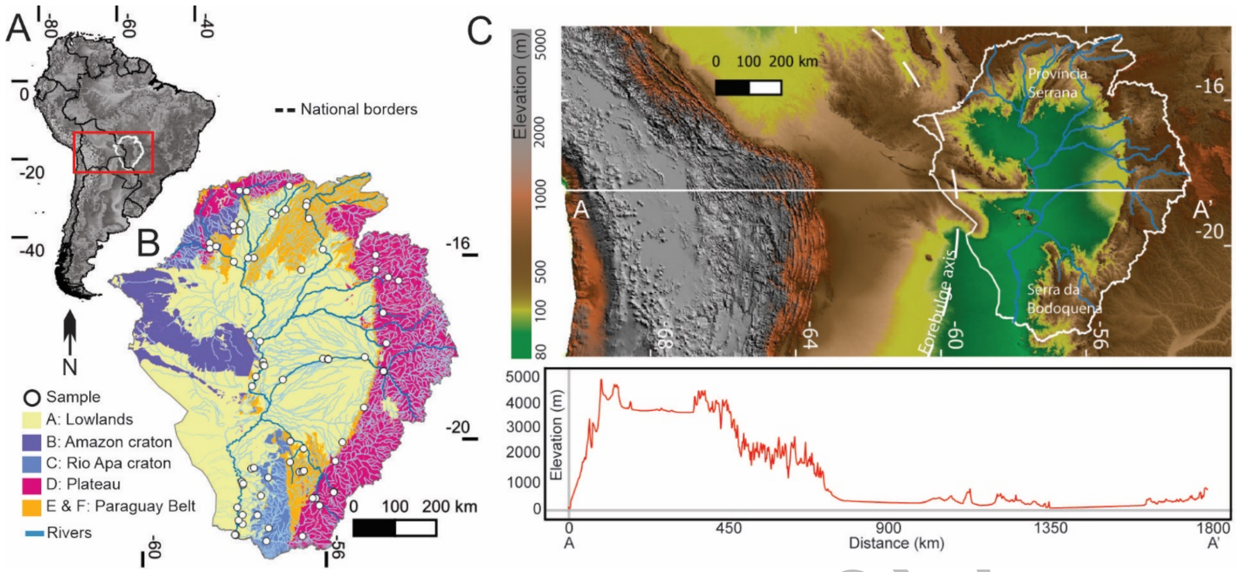

Figure 1: (A) Upper Paraguay River Basin (white outline) in South America. Red box denotes area shown in panel C. (B) Pantanal Basin provenance regions with major rivers (dark blue lines). Much of the areas covered at the surface by wetlands are designated as lowlands, in contrast with the fringing cratons and the plateau. White circles represent all sampling sites listed in Table S1. (C) GTOPO30 digital elevation model of South America (USGS, 1996), including a topographic cross-section A – A' from Google Earth©. Modified from Lo et al. (2023).

2. Geological setting of the Pantanal Basin

The Cenozoic Pantanal Basin formed from flexure of the crust as the Andes range arose from the subduction of the Pacific plate beneath the South American plate (Horton & DeCelles, 1997; Assine et al., 2016). The Pantanal Basin has accumulated ~500 m of sediment, with the depocenter located near the geographic center of the basin in the area of the Taquari River (Ussami et al., 1999). The Pantanal Basin is occupied by large distributary fluvial systems also known as fluvial megafans (Assine, 2005; Zani et al., 2012; Hartley et al., 2013; Weissmann et al., 2015). Unconsolidated sediments fill the lowlands, which span ~150,000 km^2 within the Upper Paraguay River watershed covering ~465,000 km^2 of Brazil, Bolivia and Paraguay. The Pantanal Basin can be divided into six hinterland provenance regions: lowlands, Amazon craton, Rio Apa craton, plateau, and the South and North Paraguay Belt (Lo et al., 2023) (Figure 1B). Bedrock in the northwestern Pantanal consists of Amazon craton, with granites, granodiorites, schists, and dikes of quartz-diorite and quartz-gabbro making up the bedrock (Figure 2A) (Rizzotto & Hartmann, 2012; Horbe et al., 2013; Braga et al., 2019). The Rio Apa craton in the southwestern Pantanal consists of gneisses, granites, granodiorites, amphibolites, schists, and quartzites (RadamBrasil, 1982; Alvarenga et al., 2011). The plateau region hosts Phanerozoic sedimentary rocks derived from the Paraná Basin: the Aquidauana Formation (arenites, diamictites, siltites, shales), Botucatu Formation (aeolian-sandstones), Serra Geral Formation (basalts), Caiuá Group (arenites), and Paraná Group (shales, siltites, arenites, arkose) (Lacerda Filho et al., 2004; 2006). The South Paraguay Belt hosts phyllites, schists, metarenites, quartzites, and dolomitic and calcitic marble in the Serra da Bodoquena. The North Paraguay Belt includes the Província Serrana, with phyllites, schists, limestones, siltites, and arenites (RadamBrasil, 1982). The point of highest elevation is 1260 m above sea level (m.a.s.l.) on the eastern plateau, and the lowest point is 70 m.a.s.l. at the basin outlet near the confluence of the Apa and Paraguay Rivers (Figure 1C).

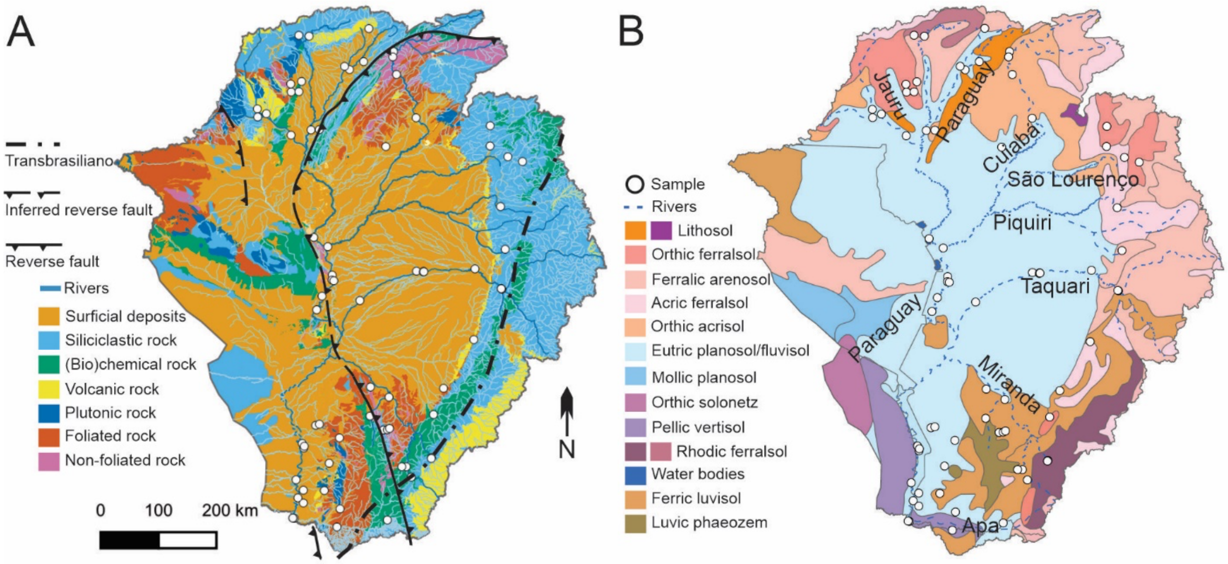

Figure 2: (A) Geology of the Pantanal Basin and drainage network, with major faults. The plateau provenance region is dominated by siliciclastic sedimentary rocks, whereas metamorphic rocks are restricted to the cratons and Paraguay Belt. (B) Soil map for the Pantanal Basin (FAO, 1971). The most widespread soil classes are eutric planosol/fluvisol in the lowlands (Benedetti et al., 2011). Geologic information was obtained for Bolivia (Dirección de Ordenamiento Territorial, Gobierno Autónomo Departamental de Santa Cruz), Paraguay (Vice Ministerio de Minas y Energía), and Brazil (Serviço Geológico do Brasil, CPRM). Faults are based on published studies (Rizzotto & Hartmann, 2012; Warren et al., 2015; Faleiros et al., 2016; Barboza et al., 2018; Rivadeneyra-Vera et al., 2019; Cedraz et al., 2020). White circles represent all sampling sites listed in Table S1. Modified from Lo et al. (2023).

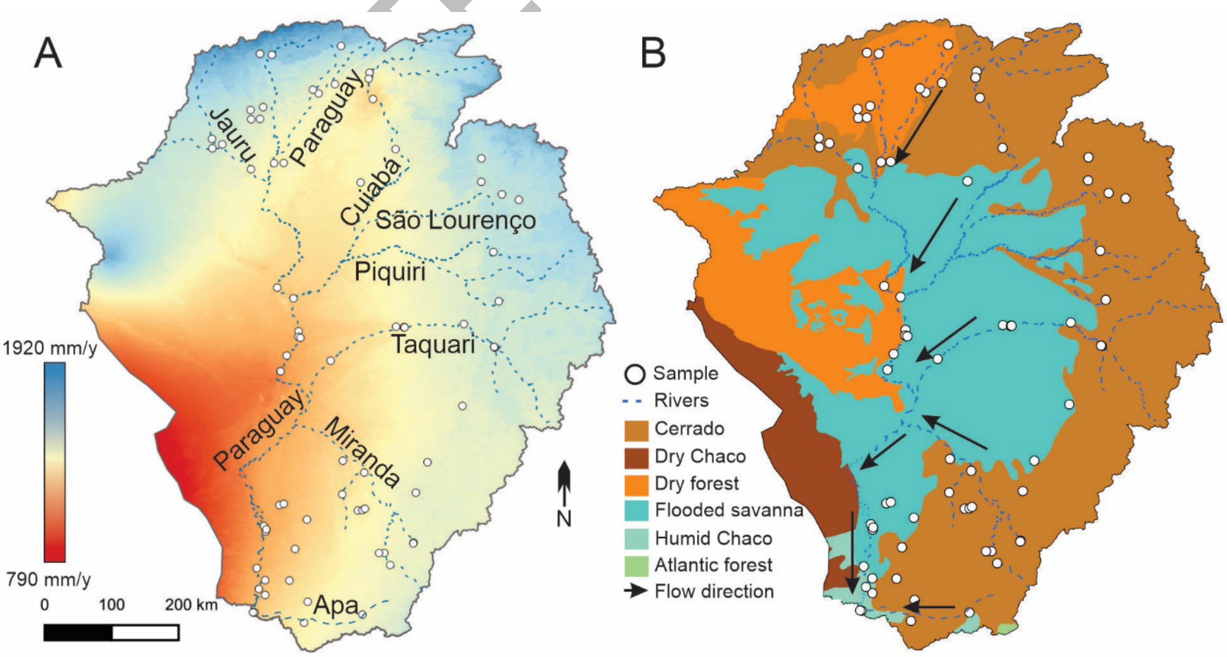

Figure 3: (A) Mean annual precipitation (mm/y) from the WorldClim database (Fick & Hijmans, 2017). In the Brazilian Pantanal, the precipitation is 970 – 1850 mm/y. (B) Vegetation ecoregions regions of the Pantanal Basin (Olson et al., 2001). The primary vegetation of the Pantanal consists of flooded savanna and *cerrado* (tropical savanna). White circles represent all sampling sites listed in Table S1. Modified from Lo et al. (Lo et al., 2023).

The hydrologic configuration of the Pantanal is responsible for the diversity of lowland environments and the contrast between wet-dry seasons (Figure 3A). The Paraguay River flows along the basin's western margin and is the trunk river of the Pantanal. The Paraguay River is joined by the Jauru River west of the Província Serrana in the North Paraguay Belt provenance region. The Cuiabá River discharges into the Paraguay River at 17.9°S latitude, followed by the Taquari River's numerous distributary channels discharging just north of 19°S latitude. The Miranda River joins the Paraguay River at ~19.4°S latitude. The Paraguay River flows along the Rio Apa craton between 21°S and 22°S latitude before flowing out of the basin. The waters that flow to the trunk river annually depend on the migration of the Intertropical Convergence Zone, which concentrates rainfall in the months of December, January, and February and strongly influences patterns of flooding and vegetation (Ivory et al., 2019). The peak dry season occurs in June, July, and August, but the dry season varies from 1 – 2 months north of the Taquari River to 4 – 5 months south of the Taquari River (IBGE, 2002). This seasonality of rainfall coupled with the minimal gradient of the lowlands results in a flood pulse effect, because rainfall in the plateau and northern Pantanal takes 2 – 3 months to flow to the basin outlet (Junk et al., 2006). When the waters rise with the flood pulse, the suspended clay particles are delivered to the riverbanks and floodplains (e.g., Hamilton, 2002). This results in broad areas of inundation in the lowlands that lasts for several months annually. Mean annual rainfall is ~1800 mm in the northern and eastern Pantanal but diminishes to ~1200 mm along the western and southern Pantanal (Figure 3A). The average annual temperature is ~25°C basinwide (Fick & Hijmans, 2017).

Clay minerals can be transformed in contemporary soils depending on climate, slope gradients, and vegetation (Hillier, 1995; Velde & Meunier, 2008) (Figures 2B and 3B). The soils of the Pantanal are dominated by eutric planosols and fluvisols in the lowlands, but the plateau provenance region is more variable (Figure 2B). The plateau region contains mostly ferralsols and arenosols in addition to luvisols in the south (Benedetti et al., 2011). Lithosols are present in the Província Serrana region, and the western Pantanal contains mollic planosols, rhodic ferralsols, and orthic solonetz. Figure 3B illustrates the general patterns of vegetation, but additional floral diversity relates to the spatial distribution of soil types (de Souza et al., 2021). Broadly, the soils are divided into forest formations, arboreal *cerrado*, herbaceous *cerrado*, chaco (woody steppic savanna), monodominant formations, and mixed vegetation (dos Santos Vila da Silva et al., 2021). For example, semideciduous (*capão*) and deciduous forests thrive in vertisols, whereas the savanna woodlands (*cerradão*) grow best in arenosols (de Souza et al., 2021).

3. Methods

3.1. Initial design and fieldwork

Paired sand and silt plus clay samples were collected from river margin bars in the Pantanal in 2019 – 2021. Sampling sites were chosen to maximize spatial coverage and lithological diversity and for ease of access. At several sampling sites (*n* = *22*), accompanying hydrologic flow data was recorded at the closest available stream gauge (Table S2). Samples were collected in both the wet and dry seasons (Table S1). Each site was treated as a pour point, which is the endpoint of a streamflow network (Gleyzer et al., 2004). Pour point analysis was completed with QGIS 3.4.6 to define each sample's contributing watershed using Shuttle Radar Topography Mission (SRTM) digital elevation models (DEMs) from USGS EarthExplorer (https://earthexplorer.usgs.gov). Pour point analysis for watersheds > 250,000 km^2 was completed with 3-arc second resolution DEM (Verdin, 2017). The average watershed slope was calculated from these DEMs, whereas elevation and distance from the Paraguay trunk river were extracted from Google© Earth. The precipitation and temperature for each sampling site were measured from WorldClim (Fick & Hijmans, 2017) (Table S1). Soils were identified in each watershed from global FAO (1971) data and converted to the United States Department of Agriculture classification for the purposes of literature review (Deckers et al., 2003; Souza et al., 2018), and vegetation ecoregions were also identified from global data (Olson et al., 2001). We did not collect local soil profiles and document local vegetation at each sampling site, because we considered each sample to be the product of cumulative upstream processes rather than localized processes and features. Geologic data were extracted from national geologic maps (Lacerda Filho et al., 2004, 2006; SERGEOMIN, 2005; Spinzi & Ramírez, 2014) (Table S3). Seventy-four (74) distinct silt plus clay sampling sites were studied, and of these, 71 samples have mineralogy data, 66 have geochemical data, and 63 have both mineralogy and geochemistry data.

3.2. Pretreatment and XRD analyses

The silt plus clay fraction was separated by wet sieving using a 53 μm sieve. We treated each sample with 1N sodium acetate (NaOAc) with pH 5 adjusted using glacial acetic acid (HOAc) to dissolve carbonates and replace the exchange sites for Ca and Mg with Na. We used 30% hydrogen peroxide (H_2O_2) to dissolve organic matter, followed by washing once with 200 mL NaOAc and 200 mL with 1M sodium chloride (NaCl) (Jackson, 1969). To obtain the <2 μm fraction, we centrifuged the samples first at 750 rpm for 3 minutes and decanted the supernatant (liquid >2.5 cm from bottom of a 250 mL bottle) containing the <2 μm clays into a separate container for settling. The bottle was refilled with sodium carbonate (Na_2CO_3) and the process repeated until a relatively clear supernatant was achieved. The remaining material was separated as the silt fraction (2 – 54 μm). Several days to weeks was allowed for the clays to settle, and 50 mL of the clays were transferred to a centrifuge tube for freeze drying (Figure 4).

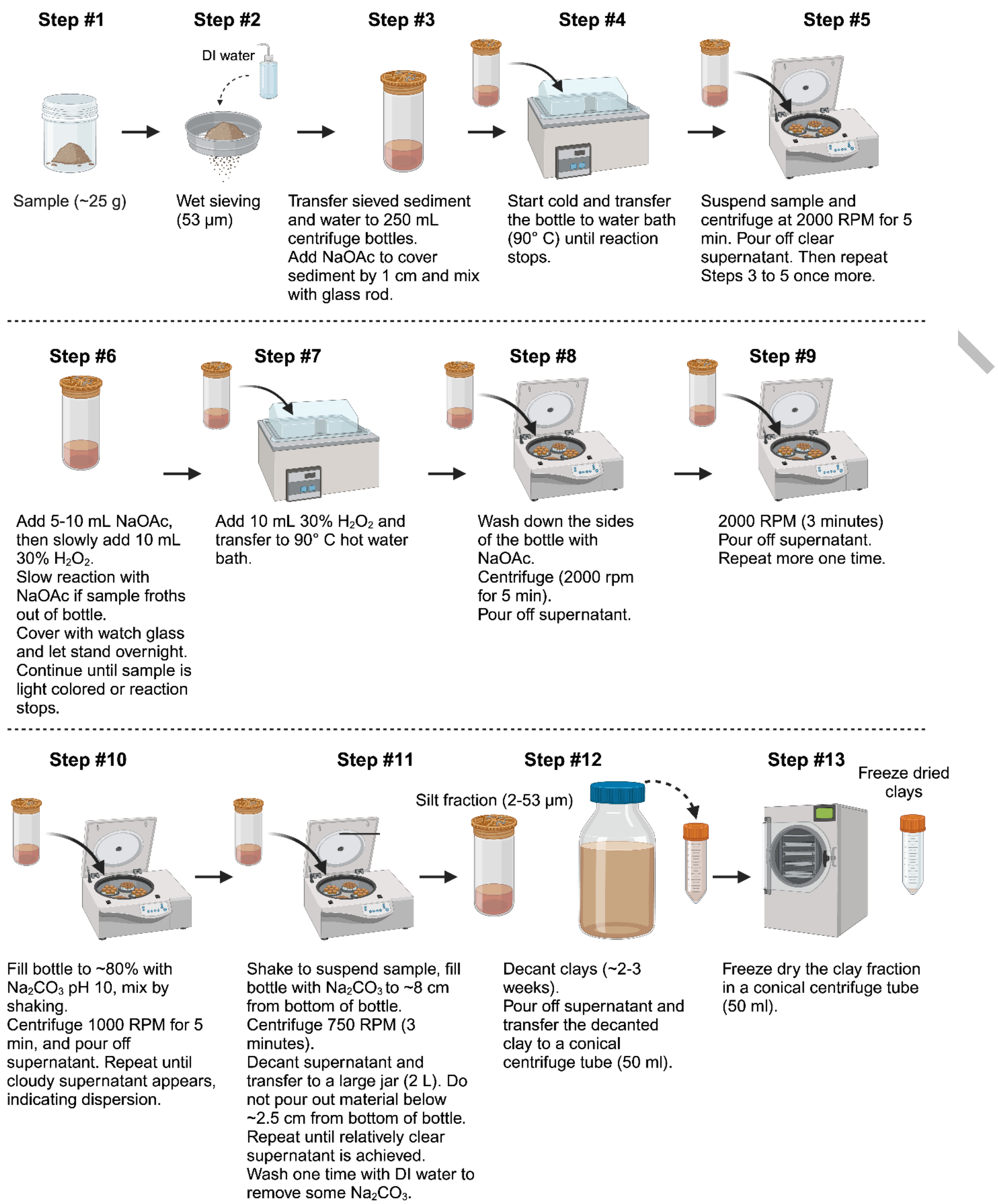

Figure 4: Flowchart created with BioRender.com that summarizes all pretreatment steps, modified from Jackson (1969). The process begins with a wet sample, dissolution of organic matter and carbonate, separation of <2 µm clays from silt (2 – 53 µm), and freeze drying of the <2 µm clays.

Oriented slides of clay fractions were prepared using the filter peel method (Drever, 1973), with diagnostic treatments of magnesium (Mg), Mg-glycerol, and a potassium (K)-saturated slide. The use of Mg-saturation and subsequent ethylene glycol is chiefly to identify smectite (Aparicio et al., 2010). The application of K-saturation is to identify vermiculite, and further heating to 550°C confirms the presence of kaolinite. Briefly, we measured 200 mg of freeze-dried clay (<2 µm) for each slide and transferred the sample to 50 mL centrifuge tubes. We added 25 mL 0.5 M magnesium chloride ($MgCl_2$), mixed well, and sonicated. In a separate centrifuge tube, we added 25 mL 0.5 M potassium chloride (KCl) to 200 mg of freeze-dried clay, mixed well, and sonicated. The tubes were centrifuged at 2000 rpm for 5 minutes, the supernatant was discarded, and the process was repeated twice more. We added deionized water, mixed, sonicated the sample, and poured the mixture onto a Millipore 0.45 µm membrane filter mounted to a vacuum flask. With the clay still moist, we removed the filter and placed the filter clay side down on a glass slide. We lightly rolled a 20 mL glass vial across the back of the filter as we peeled away the filter, leaving behind a uniformly thick oriented clay mount.

The mineralogy of the oriented clays was determined using XRD. A PANalytical X'Pert diffractometer with a Cu tube at 45 kV and 40 mA from 2° – 40° with a step size of 0.03° 2-theta (2θ) step size and scan step time of 10 seconds was employed for the analysis. Total scan time was ~3.5 hours for each treatment: Mg-saturated, K-saturated, Mg-glycol solvated, and K-saturated and heated (550°C). When the first two treatments were scanned, we solvated the Mg-saturated slide with glycol to identify if smectite was present, and the K-saturated slide was heated to 550°C for one hour to collapse the kaolinite structure. The major constituent clays identified in X-ray diffractograms used established 2θ peak positions (e.g., Moore & Reynolds, 1989). All data were analyzed using X'Pert HighScore software. Semi-quantitative calculation of clay mineral compositions was accomplished by multiplying the height (counts) by the full width at half maximum (FWHM, ° 2θ) in the Mg-saturated plot divided by the sum of the calculated areas for the predicted clay minerals and multiplied by 100 (Biscaye, 1965; Moore & Reynolds, 1989) (Table S4). These clay abundances were cross checked in NEWMOD II, in order to confirm the reliability of this semi-quantitative method (Yuan & Bish, 2010). Spatial interpolation of the three primary clay minerals (kaolinite, illite, vermiculite) was performed using the "Spline with barriers" tool in ArcGIS Pro 3.1.2. Smectite, goethite, and gibbsite were reported based on presence or absence at each sampling station. The iron content in illite was calculated using the intensity of the illite (001) and (002) peaks: I (001)/I (002) (Brown & Brindley, 1980; Deconinck et al., 1988; Furquim et al., 2010; Nascimento et al., 2015).

3.3. WD-XRF geochemistry

WD-XRF measurements completed with a Bruker AXS Inc. S4 Pioneer device were used to determine chemical elemental abundances for select bulk sediment samples (Table S5) and for the <53 µm fraction of samples with sufficient material (Table S6, *n* = *66*). Eight duplicate samples were measured to assess the repeatability of the analysis. Following the loss-on-ignition protocol, each sample was heated to 550°C for four hours to remove organic matter and 950°C for two hours to remove carbonate (Heiri et al., 2001). Samples were disaggregated and homogenized in a mortar and pestle, mixed with borate flux GF-9010 (90% lithium tetraborate and 10% lithium fluoride) in an 8:1 ratio and two drops of lithium tetraborate ($Li_2B_4O_7$), and melted into glass discs using a Katanax X-300 or K1 automatic fusion fluxer machine. The samples were calibrated with a set of eight certified reference samples using linear regression. Molar proportions were utilized to calculate the chemical weathering indices, including the chemical index of alteration (CIA; Equation 1) and the Weathering Index of Parker (WIP; Equation 2) (Parker, 1970; Nesbitt & Young, 1982).

$$CIA = \frac{100*Al_2O_3}{Al_2O_3+CaO+Na_2O+K_2O}$$ ……………………….Equation 1 (Nesbitt & Young, 1982)

$$WIP = 100*(\frac{2Na_2O}{0.35}+\frac{MgO}{0.9}+\frac{2K_2O}{0.25}+\frac{CaO}{0.7})$$ …………………Equation 2 (Parker, 1970)

Both indices are used to determine the extent of weathering (Table S6). Equation 1 (CIA) indicates the extent of feldspar-to-clay conversion, whereas Equation 2 (WIP) measures proportions of alkali and alkaline earth metals, which is suitable for weathering of heterogeneous metasedimentary lithologies (Price & Velbel, 2003). The WIP acts as an index of quartz recycling, whereas the CIA is unaffected by quartz dilution. Calculating the ratio of CIA to WIP allows us to differentiate between weathering and quartz recycling (Garzanti et al., 2019). The weathering indices were spatially interpolated using the "Spline with barriers" tool and classified using geometric intervals in ArcGIS Pro 3.1.2. We evaluated the influence of source rock composition on fine-fraction sediment chemistry using ACN, ACNK, ACNKFM plots and molar proportions of the major elements (Nesbitt & Young, 1984; Nesbitt & Wilson, 1992; Fedo et al., 1995).

We examined environmental controls on clay mineralogy and chemistry using canonical correspondence analysis (CCA). The key advantage for using CCA was to distinguish how the environmental variables and major elements affected both the clay abundance and the sampling sites. We also explored other ordination analyses to examine their effectiveness in explaining the distribution of clay minerals in the Pantanal Basin. Finally, we measured pH for a representative set of sediment samples from each region, treating each sample as a 1:2 soil/0.01 M $CaCl_2$.

4. Results

4.1. Basin-wide clay mineralogy

At basin-scale, the rank order of clay mineral abundance is kaolinite > vermiculite > illite > smectite (Table S4). Kaolinite was determined to be present if the 7 Å diagnostic (001) peak collapsed when the K-saturated slide was heated to 550°C for one hour. Illite was identified at 10 Å for the (001) peak and 5 Å for the (002) peak. Smectite was identified on the basis of the 14 Å diagnostic peak shifting to 18 Å following Mg-glycerol (Figure 5). Vermiculite was distinguishable from smectite where the 14 Å peak did not shift to 17 – 18 Å following Mg-glycerol treatment. We identified goethite at the (110) peak at 4.18 Å and gibbsite at the (002) peak at 4.85 Å (Moore & Reynolds, 1989). The Cuiabá, Taquari, and Paraguay River muds are particularly enriched in kaolinite, representing $\geq$50% of the clay mineral composition (Figure 6). Substantial in-channel compositional variability was observed in the Taquari River, which is fed by two large tributary rivers carrying 71% kaolinite and 43% kaolinite in the plateau.

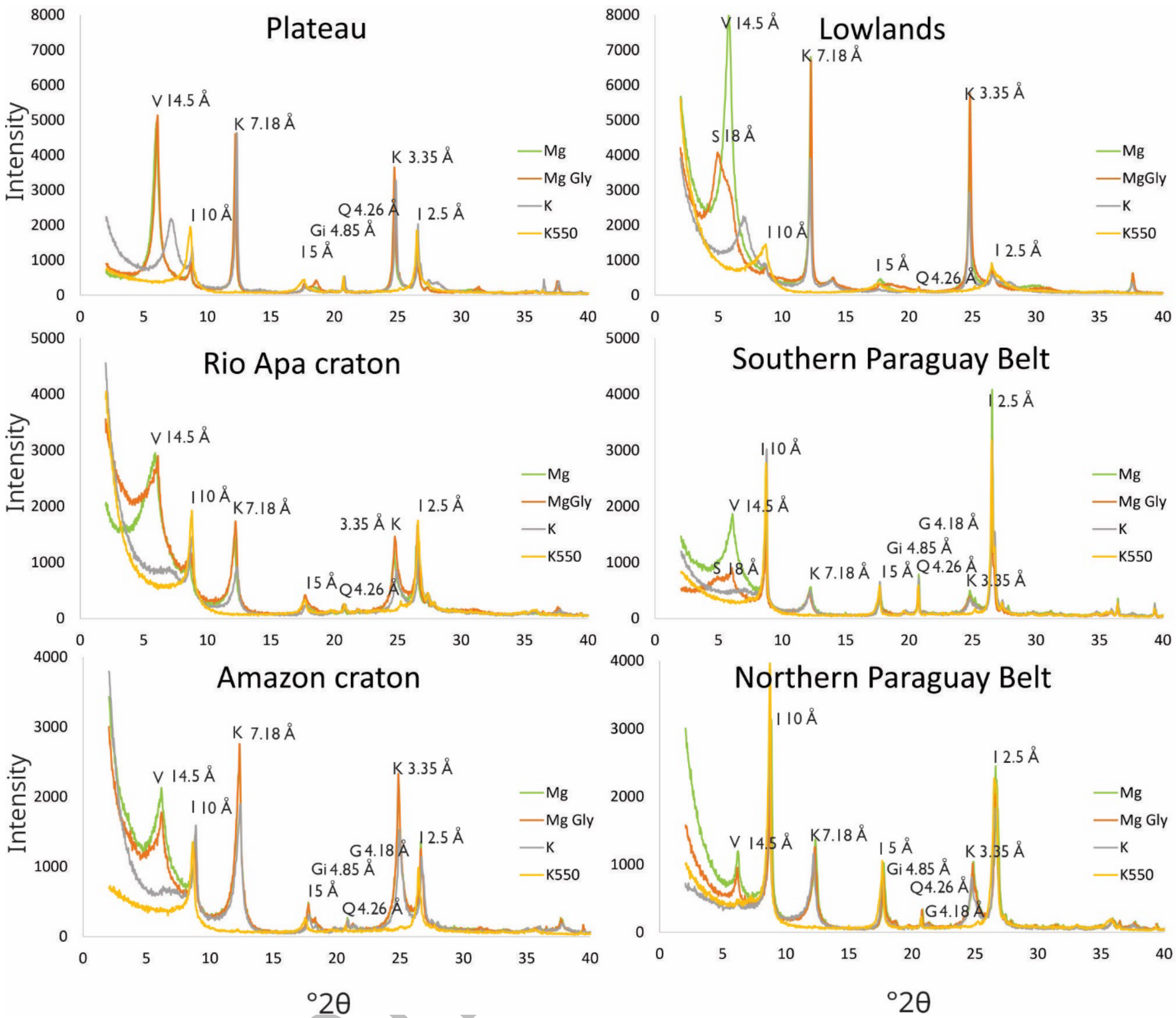

Figure 5: Representative x-ray diffractograms from oriented clay mounts using diagnostic treatments of Mg-, Mg-glycerol, K-25°C, and K-550°C for the six provenance regions detailed in Figure 1B. Diagnostic peaks are labeled for quartz (Q), kaolinite (K), illite (I), smectite (S), vermiculite (V), goethite (G), and gibbsite (Gi). The x-axis showing ° 2θ is identical across all six panels of the figure.

Spatial interpolation enabled additional basin-wide observations. The highest kaolinite percentages (>70%) were found in the medial Pantanal Basin, at the confluence of the Paraguay River with the distal distributary channels of the Taquari River (Figure 6). The medial Pantanal region is known to be regularly inundated with flood waters for some of the longest periods of the year (Ivory et al., 2019). The northernmost plateau sampling stations also produced similarly high kaolinite abundances. The northeastern plateau sampling sites were generally enriched in kaolinite downstream of orthic ferralsols and ferralic arenosols, whereas the southeastern plateau sampling sites in the Miranda River watershed with extensive ferric luvisols were depleted of kaolinite (Figures 2B and 6). In contrast, the Miranda River watershed has the highest concentrations of vermiculite in the Pantanal. As the Paraguay River flows to the basin outlet in the south, the proportion of kaolinite in the river muds decreases noticeably. There, vermiculite was more common

(>50%) in the clay assemblages, particularly at sampling sites fed by rivers draining the Rio Apa craton (Figure 6) and the South Paraguay Belt. Both the Miranda and Apa rivers drain the Serra Geral Formation dacite, which produce rhodic ferralsols (Figure 2A) (Lacerda Filho et al., 2006). Illite was 40 – 60% in the <2 μm fraction in the Paraguay Belt region where phyllite and amphibolite schist parent lithologies dominate, producing lithosols and orthic acrisols. The Paraguay Belt contained the highest contributions of illite to the Pantanal Basin, followed by the São Lourenço River draining surfaces covered by lithosols, acrisols, and ferralsols (Figures 3A and 6).

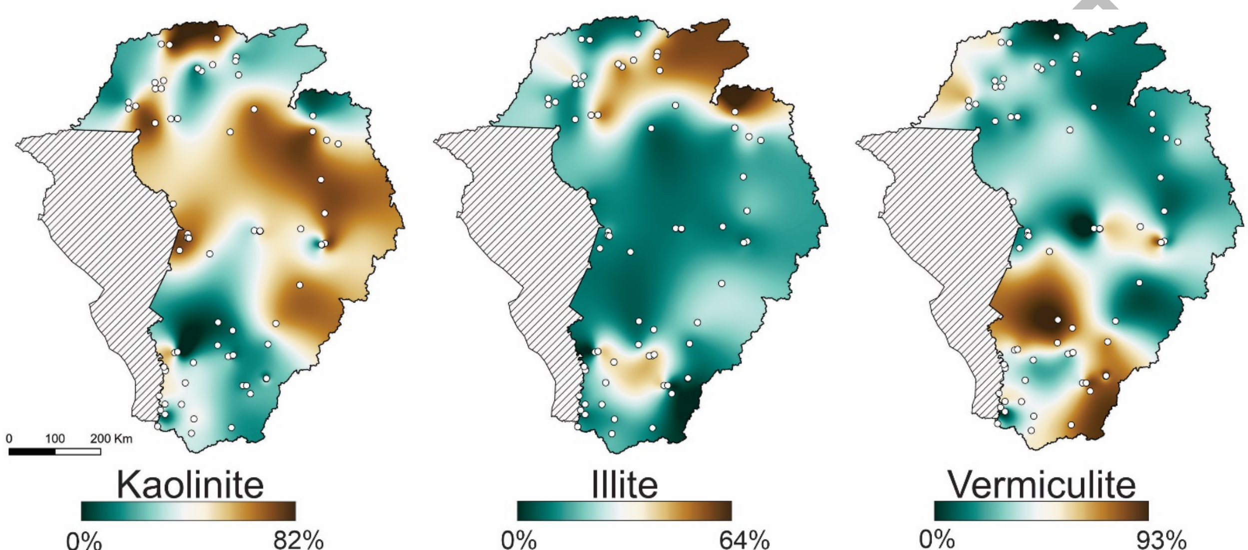

Figure 6: Spatial interpolation maps of the major clay mineral constituents at 71 sampling stations in the Pantanal. For each sampling station, the composition was normalized to 100 based on the kaolinite, illite, and vermiculite percent estimates. Interpolation was not extended to hashed areas.

The full width at half maximum (FWHM) of the diagnostic peaks shows how crystallinity changes along the length of the Taquari River (Aparicio et al., 2006). The kaolinite (001) FWHM remained constant along the length of the megafan, indicating no changes to the crystallinity. The gibbsite diagnostic peak at 4.85 Å in the Taquari River sampling station disappears from the proximal to the distal megafan regions. Chlorite was not found, and smectite was identified only at limited sites such as sample A26 in the medial Taquari River megafan where the vermiculite and smectite peaks could be clearly disentangled. The average iron content in illite was 2.19 (dimensionless, computed intensity (001)/intensity (002)), with much of the highest iron content located in tributaries of the Jauru, Paraguay, and Cuiabá Rivers in the northern Pantanal.

Gibbsite and goethite are not abundant clay minerals in samples from the Pantanal (25% of samples contained neither of these minerals), but they do constitute important minor components (Figure 7). Sampling sites with both gibbsite and goethite were most frequently present in the north plateau region, where the mean annual precipitation in the basin is the greatest (Figure 3A). Gibbsite was most common in samples along the Taquari River megafan, whereas goethite occurred in samples from the southern plateau and in the medial lowlands (Figure 7A). Samples with neither mineral were common in the Rio Apa craton in southern Pantanal. Smectite was identified in ~30% of the 71 sampling stations (Figure 7B). The presence of smectite appeared to be distributed across the Pantanal Basin with no specific pattern.

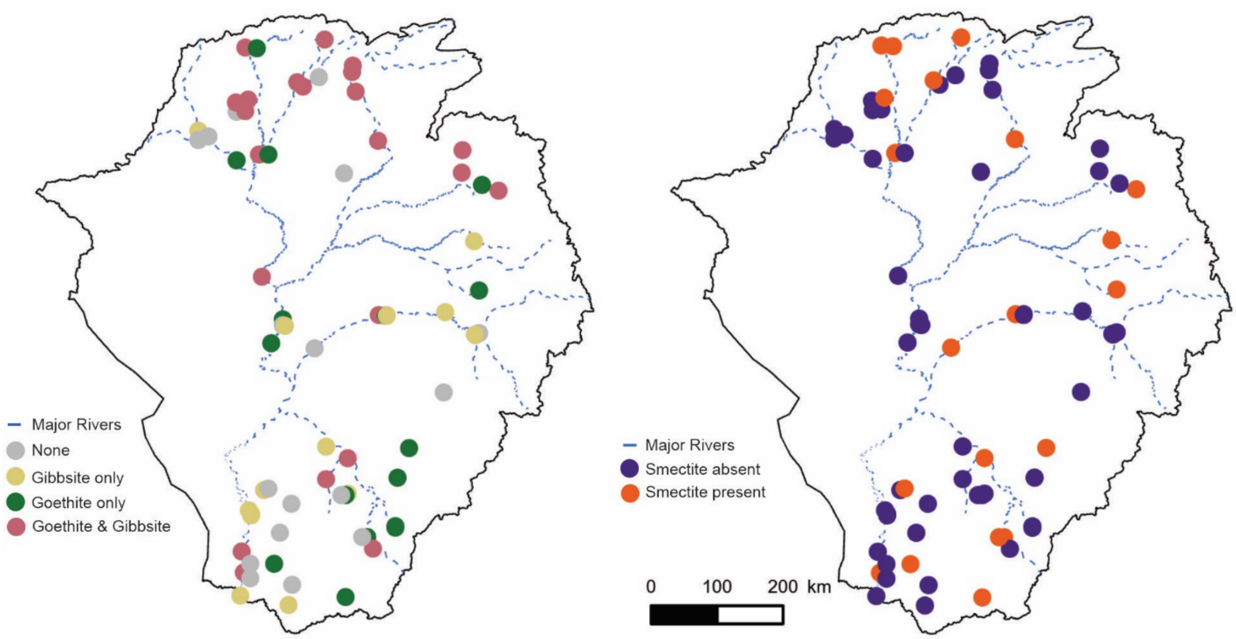

Figure 7: (A) Basin-wide map of gibbsite and goethite among 71 stations. Pink (gibbsite + goethite), green (goethite), yellow (gibbsite), and gray (neither). (B) Map of smectite in the Pantanal marked as purple (no smectite) or orange (smectite present). These maps did not account for the intensity or crystallinity of the mineral peaks.

4.2. Basin-wide geochemistry

Ternary diagrams showed that most samples exhibited >70% Al_2O_3, and all lowland samples >80% Al_2O_3 (Figure 8A, B). Most samples contained <10% Na_2O (Figure 8B) and 20-30% Fe_2O_3 + MgO (Figure 8C). Geochemically, all samples from watersheds in the South Paraguay Belt provenance region and select samples from the Rio Apa craton provenance region were enriched in Ca, Na, and K and low in Al (Figure 8C). Average values for geochemical variables in the six provenance regions further show the greatest SiO_2 enrichment in the lowlands provenance region and the least SiO_2 enrichment in the South Paraguay Belt (Table 1). The South Paraguay Belt and plateau provenance regions had average pH 6.6 and 53% kaolinite, whereas the lowland provenance region and the North Paraguay Belt had an average pH of 5.8 and 22% kaolinite (Table 2).

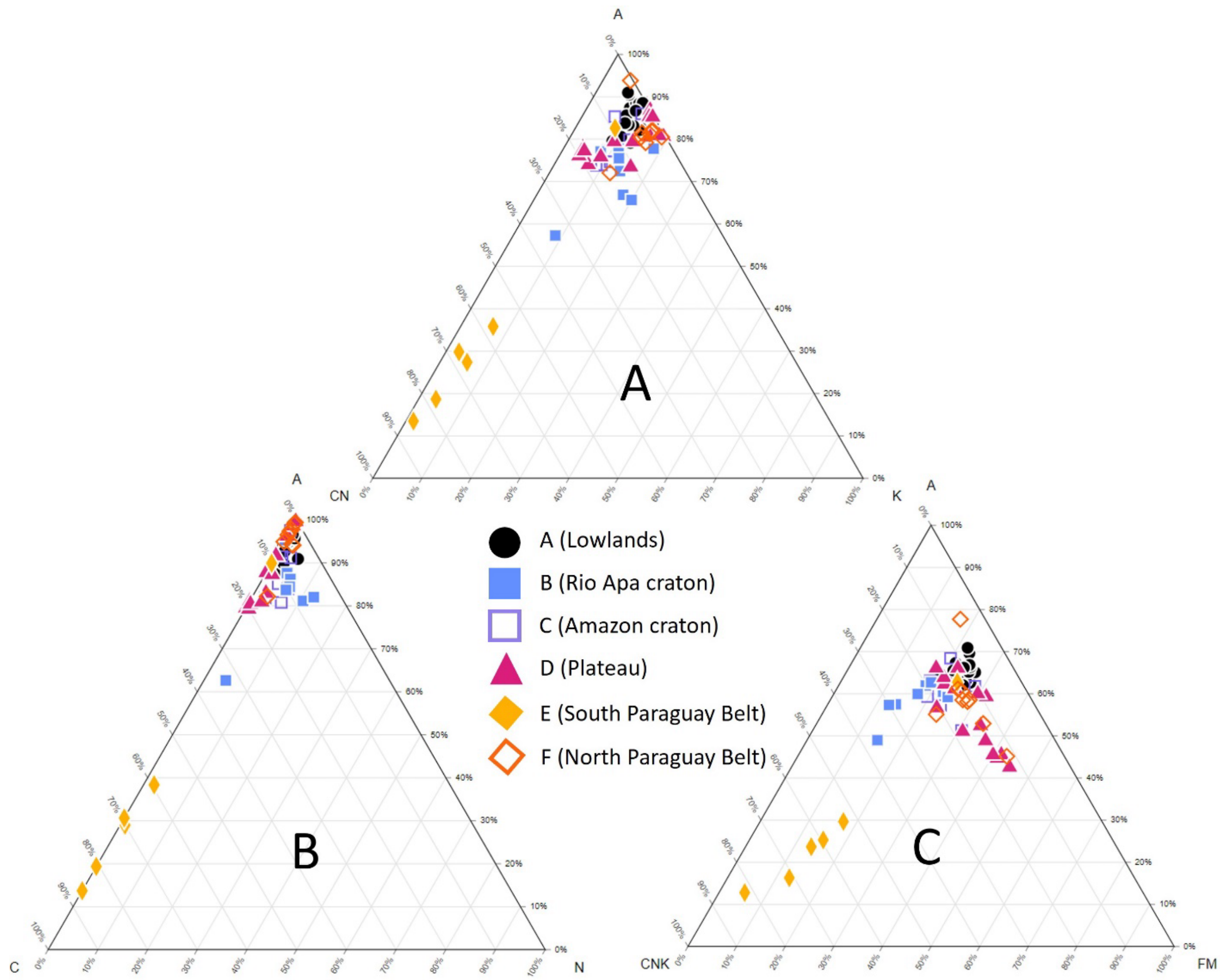

Figure 8: Major elemental compositions of fluvial sediments (*n = 66*) plotted as molar proportions on Al_2O_3-CaO-Na_2O (ACN), Al_2O_3-(CaO + Na_2O + K_2O)-(Fe_2O_3 + MgO) (ACNKFM), and Al_2O_3-(CaO + Na_2O)-K_2O (ACNK). The ACN and ACNK plots form a linear distribution with South Paraguay Belt samples closer to the C- and the CN-pole, respectively. Most mud samples rich in non-mobile Al plot closer to the A-pole. The ACNKFM plot helps distinguish the Mg-rich samples.

The geochemical discrimination plots show decreasing Al_2O_3 as SiO_2 increases, consistent with quartz addition relative to the UCC standard (Figure 9) (Taylor & McLennan, 1995). The lowland, Rio Apa craton, and Amazon craton samples followed this quartz enrichment trend closely, whereas the plateau and Paraguay Belt samples diverged from this quartz enrichment pattern. Approximately 50% of the samples (Figure 9C) contained less SiO_2 than the UCC and were mostly <5 $Na_2O+K_2O+MgO+CaO$. Most samples followed the quartz addition trend (Figure 9C, D). However, the CIA/WIP plot showed mostly a weathering trend concentrated at 70 – 90 CIA and <40 WIP (Figure 9B).

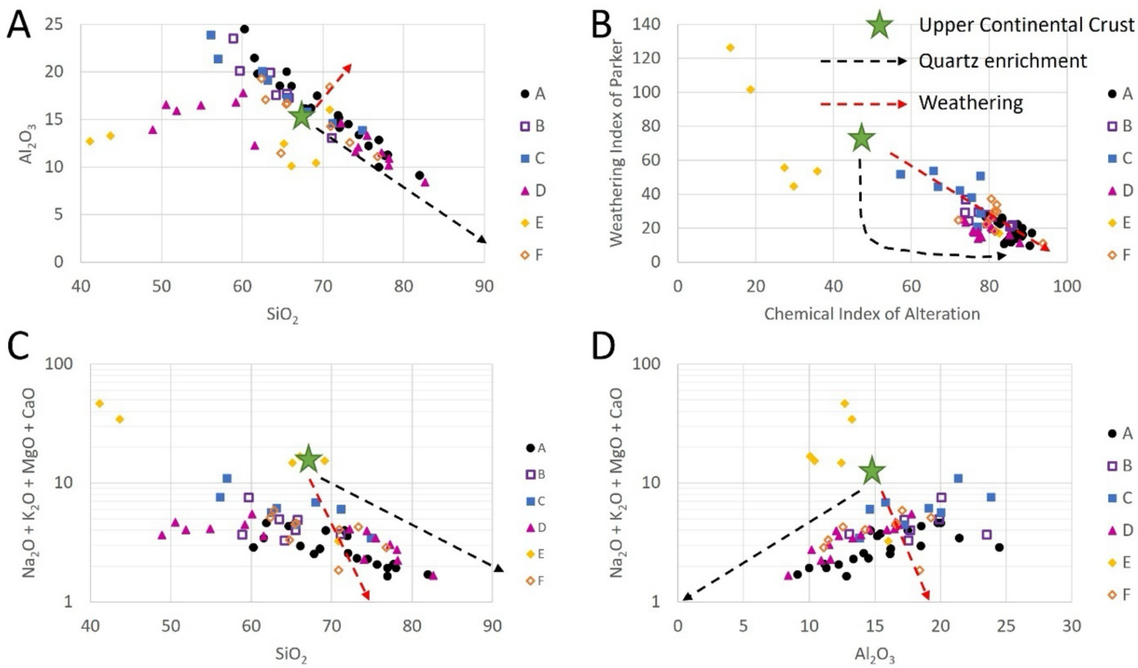

Figure 9: Geochemical discrimination plots are useful to separate effects of weathering and quartz recycling relative to the upper continental crust (UCC; green star) standard (Taylor & McLennan, 1995). Quartz addition is interpreted as the progressive addition of SiO_2, and chemical weathering is the progressive removal of mobile metals assuming Si and Al are immobile (Garzanti et al., 2010, 2011, 2012). The Al_2O_3/SiO_2 plot shows quartz enrichment patterns for about half of the samples. The two lower plots suggest weathering control and only weak quartz enrichment. All regions here are consistent with the areas defined in Figure 1. The quartz enrichment and weathering trends are approximate in C and D due to the logarithmic scale on the y-axis. The legend is identical to that of Figure 8.

Table 1: Chemical elemental abundance summary statistics

Provenance Area	SiO_2 wt%	Al_2O_3 wt%	Fe_2O_3 wt%	K_2O wt%	Na_2O wt%	CaO wt%	MgO wt%	Kao	Illite	Verm	CIA	WIP
A Lowlands	71.8	15.0	5.6	1.7	0.1	0.4	0.8	**56**	**5.6**	**35**	85.0	18.0
	Comments: kaolinite comprised 50 – 60% of the Paraguay River clays near the basin outlet. Vermiculite composed >30% of the lowland clays downstream of the Rio Apa craton.											
B Amazon craton	64.1	18.4	7.4	2.1	0.4	1.1	0.9	**51.3**	**16**	**32.6**	78.7	27.2
	Comments: vermiculite varied 15 – 59%, and illite ranged 7 – 36%.											
C Rio Apa craton	64.8	18.2	5.7	3.3	0.8	1.5	0.8	**31.4**	**18.9**	**38.8**	71.3	41.2
	Comments: smectite was common where volcanic rocks formed 16% of the watershed. Kaolinite was most common in the sample where foliated metamorphic rocks were the single largest constituent lithology.											
D Plateau	66.6	13.5	9.5	1.6	0.1	1.0	0.9	**41.5**	**12.1**	**46.7**	79.4	19.2
	Comments: Clay assemblages in the Miranda River watersheds were almost dominantly vermiculite. Two sampling stations may drain the same siliciclastic lithologies but produce vastly different proportions of kaolinite, for example.											
E South Paraguay Belt	59.3	12.5	5.5	1.7	0.1	18.7	1.3	**18.5**	**30.3**	**51.2**	34.6	66.4
	Comments: kaolinite reached the lowest proportions of any area in the Pantanal. Biochemical lithologies were the main parent rock of the watersheds, but clay assemblages were more commonly controlled by the adjacent metamorphic lithologies.											
F North Paraguay Belt	68.1	15.3	7.2	2.5	0.1	0.3	1.1	**37.3**	**42.6**	**20.2**	81.4	25.8
	Comments: many simples contained >50% illite, which exceeds all other regions in the Pantanal.											

Note. Provenance regions are lowlands (A), Amazon craton (B), Rio Apa craton (C), plateau (D), South Paraguay Belt (E), and North Paraguay Belt (F). Average smectite values were not determined due to occurrence in few sampling sites. Abbreviations are Kao = kaolinite and Verm = vermiculite.

Table 2: pH values for selected samples

Sample	pH	%Kaolinite	Kaolinite FWHM
A2	5.34	57	0.3542
A3	5.40	51	0.4723
F2	5.86	34	0.4723
F1	5.88	73	0.3542
C1	5.94	39	0.3542
C8	5.97	39	0.3542
A27	5.98	52	0.3542
B1	5.99	77	0.3542
C2	6.33	5	0.3542
D1	6.37	25	0.3542
B2	6.58	56	0.3542
E1	6.62	17	0.4723
E3	6.82	15	0.2952
D3	6.85	12	0.3542

Note. Samples are ordered by increasing pH representing the six provenance regions: lowlands (A), Amazon craton (B), Rio Apa craton (C), plateau (D), South Paraguay Belt (E), and North Paraguay Belt (F). The sample with the largest watershed in each provenance region was chosen to obtain the net cumulative pH value.

4.3. Weathering indices and statistical analysis

Table 1 provides summary statistics across all six provenance regions. The CIA and WIP values showed that samples from the lowlands provenance region were the most weathered, especially near the Taquari megafan where high values (83 – 94) of the CIA were recorded. Weathering intensities measured by WIP were more variable in the lowlands (10 – 36) (Figure 10). The Itiquira and Piquiri Rivers draining the plateau highlands immediately north of the Taquari River produced silt plus clay minerals that were consistently highly weathered as indicated by the CIA and WIP. The weathering indices reflected the clay mineral proportions deduced by XRD; the areas with the greatest kaolinite proportions coincided with the highest CIA values and the lowest WIP values for the Piquiri, Cuiabá, São Lourenço, and the Paraguay River at the Taquari megafan (Figure 10). In contrast, the lowest CIA values and highest WIP values were recorded in the Rio Apa and South Paraguay Belt regions (Figure 10).

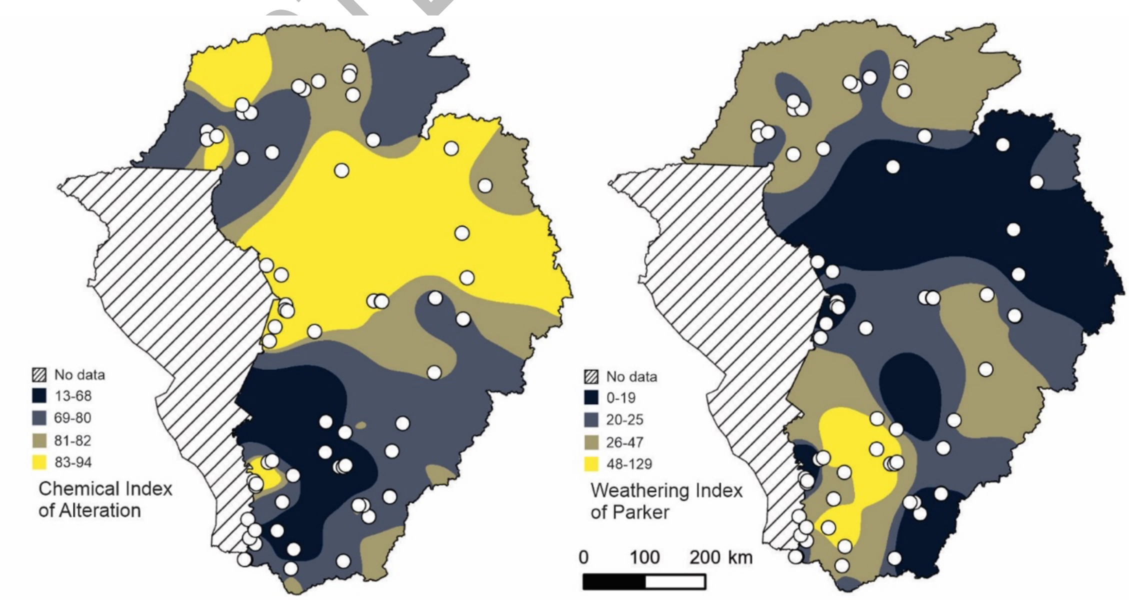

Figure 10: Spatial interpolation maps of chemical weathering indices based on the molar proportions of the major elemental data from 66 sampling stations.

Fe_2O_3 and metamorphic parent lithologies loaded positively on axis 1 of the canonical correspondence analysis (Figure 11). The SiO_2, K_2O, and average watershed slope loaded negatively on axis 1. The average watershed slope, MgO, and Fe_2O_3 loaded positively whereas watershed area, sedimentary parent rocks, and SiO_2 loaded negatively on axis 2. All lowland samples plotted in negative axis 2 space, whereas most of the Paraguay Belt samples plotted in positive axis 2 space. Two large clusters of data points are distinguishable. The first cluster is oriented diagonally along a continuum formed by the SiO_2 and Fe_2O_3 rays with *n = 44* sampling sites. The samples with more SiO_2 are also closer to the abundance of kaolinite, and samples with more Fe_2O_3 are associated with vermiculite. The quadrant with vermiculite is characterized by significantly more MgO and slightly more Al_2O_3, as suggested by the length of the shorter ray for Al_2O_3. The second cluster of data is oriented perpendicular to the first cluster, composed mostly of Paraguay Belt samples and an association with illite, K_2O, average watershed slope, and elevation of the sampling stations.

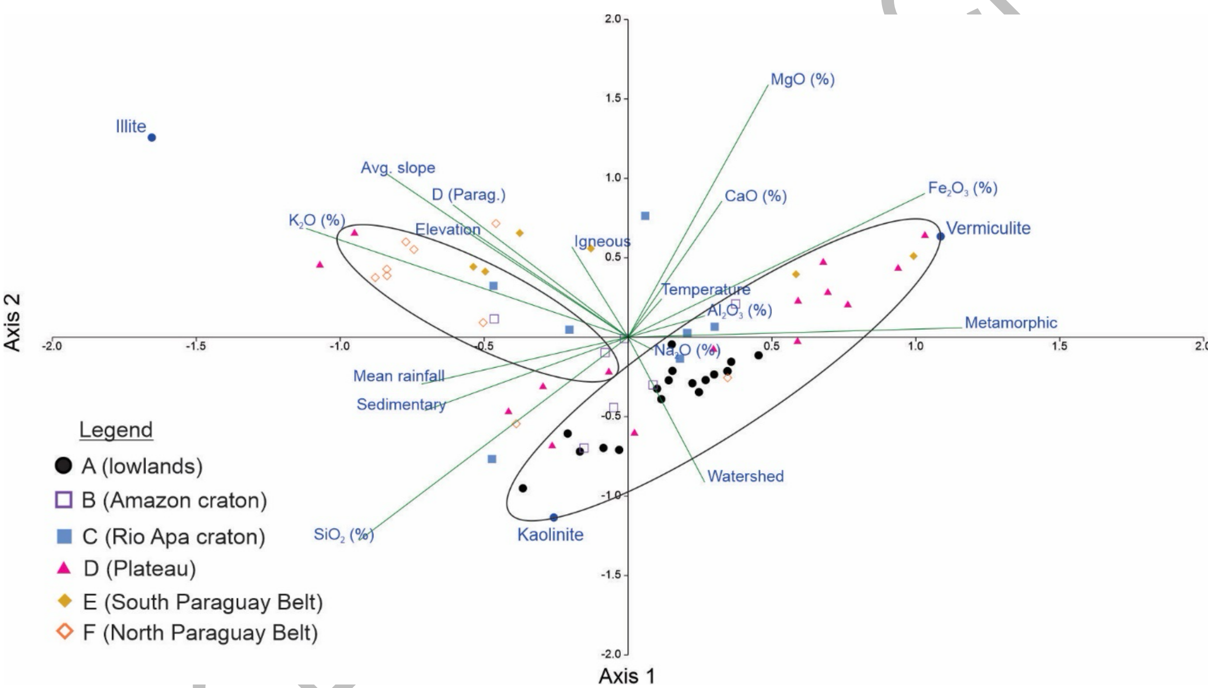

Figure 11: Canonical correspondence analysis shows that the South and North Paraguay Belt areas are enriched in K_2O, whereas the sampling stations in the Miranda River basin in the plateau region are enriched in Fe_2O_2 in the first axis. In the second axis, most of the Rio Apa craton and Paraguay Belt sampling stations show enriched MgO and CaO.

5. Discussion

5.1. Insights from clay mineralogy

5.1.1. Climate control

The Pantanal Basin is warm and seasonally wet with open *cerrado* savanna vegetation in the hinterland areas (Cole, 1960), where a pronounced hydroclimate gradient in rainfall and seasonality controls modern clay distribution. The Taquari River forms a weathering hinge between the increased weathering intensity to its north and reduced weathering intensity to its south. The greater rainfall and shorter dry season north of the Taquari River results in high kaolinite production as bedrock and soils are leached (Goldich, 1938;

Depetris & Griffin, 1968; Singer, 1980; Garzanti et al., 2014; Guinoiseau et al., 2021). Most neoformed kaolinite in soils is subsequently transported downstream towards the Paraguay River in the suspended sediment fraction (e.g., Depetris & Probst, 1998). The fluvial sediment samples in the medial Pantanal reflect the cumulative climate-driven weathering north of the Taquari River hinge. On the basis of greater kaolinite abundance in the northern Pantanal, our data broadly support the hypothesis that mean annual precipitation controls clay mineralogy.

As the clay minerals are carried as suspended loads, their composition is subsequently transformed (Setti et al., 2014). Detrital clays such as vermiculite and illite can be compared with transformed clays such as kaolinite and smectite as a measure of chemical weathering and mechanical erosion (Shover, 1963; Vanderaveroet et al., 2000; Setti et al., 2014). The Jauru and Paraguay River clays west of the Província Serrana are mostly kaolinite, plus illite from the North Paraguay Belt. These clays likely originated from the Amazon craton and the Paraguay Belt lithologies, in addition to the siliciclastic plateau at the northernmost end of the basin. The illite (> 60%) in the uppermost Cuiabá River and along small watersheds of the North Paraguay Belt points to rapid mechanical weathering (e.g., Selvaraj & Chen, 2006). Mechanical weathering breaks down outcrops of the muscovite-bearing Cuiabá Group rocks (Alvarenga et al., 2011; Vasconcelos et al., 2015). This interpretation is consistent with the lithosols, which are thin and poorly developed (Camargo & Bennema, 1966). Following the confluence with the Cuiabá River, the Paraguay River carries more kaolinite, similar to levels recorded in the tributaries of the Cuiabá River.

Lower kaolinite proportions in samples from sites south of the Taquari River are interpreted to be linked to reduced rainfall (~1200 mm/y) and increased length of the dry season (4 – 5 months). In contrast, areas north of the Taquari River are characterized by ~1800 mm/y and 1 – 2 month-long dry season. This pattern of reduced weathering intensity that produces more detrital clays (e.g., illite and vermiculite) relative to transformed clays (e.g., kaolinite and smectite) supports our hypothesis.

The 2:1 type clays were primarily vermiculite, commonly a byproduct of incomplete weathering of biotite (Cleaves et al., 1970; Ojanuga, 1973; Johnsson & Meade, 1990). The Paraguay River clays downstream of the confluence with the Taquari and Miranda Rivers begin to incorporate substantial vermiculite. The South Paraguay Belt region and the plateau provenance region south of the Taquari River weathering hinge contain ferric luvisols overlying carbonate and foliated metamorphic rocks, a unique combination of geological factors in the Pantanal Basin. As the Paraguay River flows along the Rio Apa craton towards the basin outlet at the confluence with the Apa River, the clay composition is modified by the illite and vermiculite chemically and mechanically eroded from the craton. The intensity of weathering inferred from the relative proportions of 50% kaolinite and 50% illite + vermiculite would indicate incomplete weathering closer to the outlet (samples A2 and A3; Table S1) than in the medial Pantanal Basin (samples A6 – A9; Table S1). The modification of the Paraguay River suspended clays attests to non-linear compositional changes downstream.

5.1.2. Soil control

The composition of extant soils in the provenance regions is interpreted to be an important secondary control on modern clay mineralogy and chemistry. Although we did not examine the mineralogy of soil profiles adjacent to each sample, we can infer soil properties and clays based on the soil classification map (Figure 2B). Using the soil classification map is sufficient for this study, because each sample is an integrated result of the cumulative processes in the entire upstream watershed.

The extensive availability of kaolinite in the dominant soils helps to explain higher proportions of kaolinite in modern fluvial samples north of the Taquari weathering hinge. Soils in the northern Pantanal Basin were described as acrisols, arenosols, and ferralsols. The acrisols and ferralsols are known to have high amounts of kaolinite and gibbsite clays in the topsoil and subsoil, whereas the arenosols contain kaolinite and illite primarily in the subsoil (Ito & Wagai, 2017). The abundant kaolinite usually occurs in lateritic soils (e.g., Truckenbrodt et al., 1991), which may appear as ferralsols or ferralic arenosols in the Pantanal (Figure 2B) (Righi & Meunier, 1995; Mathian et al., 2020). Some of the kaolinite formed from laterite is instead replaced by hematite (Ambrosi et al., 1986), as observed by the iron-rich concretions (~1 cm in diameter) on the armored, wind-deflated surface of the Taquari River's lateritic soils (Figure 12). Although not shown on the map, gleysols and plinthosols also contribute to the high occurrence of kaolinite in the northern Pantanal soils (Coringa et al., 2012).

Soils in the southern Pantanal Basin are distinguished by the extensive development of luvisols that contain greater proportions of illite in both the topsoil and subsoil (Ito & Wagai, 2017; Warr, 2022). The South Paraguay Belt soils are dominantly mollisols, containing primarily vermiculite, followed by illite (Warr, 2022). Mollisols are interpreted as key contributors to the higher proportions of vermiculite in the southern Pantanal. Soil clay mineralogy and the processes may be altered due to human-induced land use changes (e.g., Céspedes-Payret et al., 2012; Fink et al., 2014; Austin et al., 2018). However, the relationship between land use and fluvial clay minerals remains unclear, so disentangling the anthropogenic land use effect on clays from each sample is not feasible. The presence of gibbsite is an indicator of intense weathering and desilication (Certini et al., 2006; Reatto et al., 2008). Gibbsite is an aluminum hydroxide associated with strong hydrolysis and bauxitization processes (Chamley, 1989; Velde & Meunier, 2008). Bauxitization, or the formation of aluminum ore, occurs when extensive hydrolysis leads to gibbsite authigenesis. We infer that the gibbsite was eroded primarily from the surrounding soil cover (phaeozems, luvisols, and ferralsols). The northeastern Pantanal including the São Lourenço and Cuiaba Rivers are sources of gibbsite. Gibbsite peaks were also identified in the Amazon craton rivers and the South Paraguay Belt samples. The gibbsite identified in the medial Paraguay River, upstream of the confluence with the Taquari River, were likely derived from erosion of lateritic soils in the uppermost regions of the plateau provenance region. Iron-bearing minerals, particularly hematite and goethite, are common in lateritic soils (Madeira et al., 1997). However, the occurrence of gibbsite and goethite was not consistently related to higher or lower kaolinite proportions. This observation suggests that the highest proportions of kaolinite are independent of goethite and gibbsite occurrence.

Figure 12: Uppermost hinterland of the Taquari River watershed consists of (A) deeply incised gullies facilitating sediment export to the lowlands. The surfaces are commonly characterized by friable iron-rich concretions, known as ferricretes (B, C, D). Photo credit: E. Lo.

5.1.3. Geological and slope control

When illite is generated from metamorphic rocks, rapid removal of material is often implicated, which is expected in a tropical environment with heavy seasonal rainfall like the Pantanal (Selvaraj & Chen, 2006; Velde & Meunier, 2008; Wang et al., 2011). The close spatial relationship between illite abundances and the North and South Paraguay Belt provenance regions suggests a direct contribution from the muscovite-rich greenschist facies (Almeida et al., 1976). The broad spatial occurrence of illite in the North Paraguay Belt region is evidence of mechanical bedrock erosion observed in regions of high precipitation (e.g., Liu et al., 2012). Calculation of iron content in the mica structure yielded a relatively high dimensionless average value of 2.19 (dimensionless, computed intensity (001)/intensity (002)) (Brown & Brindley, 1980; Deconinck et al., 1988). High iron availability is a prerequisite for authigenesis of ferric illite (Furquim et al., 2010), consistent with tropical environments that generate extensive iron oxides (Liptzin & Silver, 2009). The largest values for Fe content in the illite were mostly concentrated north of the Taquari weathering hinge. The increased distribution of illite in the North Paraguay Belt is consistent with present-day weathering conditions.

The weathering of phyllite and amphibolite schist outcrops along the Salobra River, the Miranda River, and the uppermost Apa River are the best candidates for vermiculite generation. Select sampling stations in the Miranda River contain as much as 90% vermiculite, which we attribute to the erosion of adjacent Cuiabá Group phyllites (Lacerda Filho et al., 2006). Dacites such as the Serra Geral Formation in the study area have generated vermiculite clays in other regions (Harvey & Beck, 1962). Illite may also be altered to vermiculite as K is released in the soils, creating an interlayered illite-vermiculite mineral similar to Amazon Basin soils and verified with NEWMOD II fitting (Han et al., 2014; Delarmelinda et al., 2017). Sample E1 in the South Paraguay Belt region contained an intermediate peak at 11.9 Å suggesting the presence of hydroxy-interlayered vermiculite (HIV), implicating a mixed layer illite-HIV.

The average watershed slope regulates fluvial incision and channel behavior. Steeper slopes favor higher mass wasting rates, incised river channels, and minimal pedogenic development. In contrast, the low-slope floodplains act as temporary sinks for unconsolidated, highly weathered fine sediment subject to fluvial channel migration. The Taquari River at the distal Zé da Costa avulsion (sample A25; Table S1) contained greater amounts of vermiculite than at the medial Caronal avulsion (samples A26-A27; Table S1), suggesting that reworked floodplain sediments may be an important contribution of vermiculite in the distal Taquari River. The exhumation of floodplain deposits can remobilize clays that were deposited during drier Holocene climatic conditions where transformation of clays was less efficient (McGlue et al., 2015, 2017; Novello et al., 2017). Vermiculite is diluted by dominantly kaolinitic tributary inputs when the Taquari River discharges into the Paraguay River.

Clay minerals may represent inherited weathering phases from recycling of more ancient sedimentary rocks that are exhumed to the surface environment (Eberl et al., 1997; Wilson, 1999; Bhattacharyya et al., 2000). For example, inherited clays may come from clay coats that formed prior to lithification of aeolian sands into arenites (Wilson, 1992). The Mesozoic Botucatu Formation in the plateau provenance region is an aeolian sandstone with amorphous silica, pore-filling, and kaolinite and smectite grain coatings (França et al., 2003; Hirata et al., 2011; Bertolini et al., 2020; 2021). The Mesozoic Era was characterized by hothouse conditions (Holz, 2015) followed by diagenetic processes that contributed to the generation of kaolinite in the Botucatu Formation (Corrêa et al., 2021). This formation may have contributed an unknown amount of inherited kaolinite to the silt plus clay fraction recovered in modern river samples (Balan et al., 2007). Inherited kaolinite is commonly more ordered than neoformed kaolinite (Balan et al., 2007; Bauluz et al., 2008), such that higher crystallinity with lower FWHM can indicate inheritance. Samples with the most disordered (neoformed) kaolinite (FWHM 0.45 ° 2θ) were located at the confluence of the Taquari and Paraguay Rivers, where elevations are very low and the annual floodwater inundation period is high (Ivory et al., 2019). Furian et al. (2002) likewise encountered kaolinite in poorly drained areas of the Pantanal. The high levels of kaolinite at the confluence of the distal Taquari River and the Paraguay River further attest to kaolinite authigenesis associated with strong hydrolysis (Chamley, 1989). Estimating inherited versus neoformed kaolinite remains challenging, because studies such as Balan et al. (2007) examined these processes primarily in soil profiles, not in modern fluvial samples.

5.2. Insights from geochemistry

Clay minerals generated today across the Pantanal Basin are controlled primarily by climate-induced chemical weathering and secondarily by soil and parent lithology. Nearly all Rio Apa craton samples were relatively enriched in Na, K, and Al compared to samples from rivers draining the other provenance regions. Similarly, the Amazon craton samples had high relative Na, K, and Al, but less than that of the Rio Apa craton samples. South Paraguay Belt samples were all enriched in Fe and Ca. Most of the lowland samples were high in Si, reflecting the quartzose nature of muds where repeated cycles of flooding and channel avulsions enhance sediment reworking (e.g., Louzada et al., 2021). The rivers draining provenance regions with the lowest CIA values were the Rio Apa craton and the South Paraguay Belt, suggesting that the weathering effect for these metamorphic and carbonate rocks was low, most likely due to the reduced mean annual rainfall (~1200 mm/y) (Fick & Hijmans, 2017). These two regions also had WIP >40, indicating reduced quartz recycling relative to the other four provenance regions. Most samples from the Pantanal had CIA 75 – 95 and had WIP <20, attesting to both high quartz recycling and extensive weathering effects (Figure 9B). Our spatial distribution maps show that this effect was most concentrated in the medial Pantanal Basin, supplied mainly by the Cuiabá, São Lourenço, and Piquiri Rivers (Figure 10). Maximum quartz recycling and weathering effects were consistent with the highest quartz compositions observed in Paraguay River fine fraction samples (n = 7) near the confluence of the Paraguay River with the Cuiabá and Taquari Rivers. The lowest WIP values in the basin are likely linked to the Cretaceous Botucatu Formation and the Cretaceous Bauru Formation quartz arenites of the plateau provenance region (Fernandes & Magalhães Ribeiro, 2015; Bertolini et al., 2021). Because quartz arenite weathering contributes little to the clay fraction in extant river muds, we interpret that most of the depletion of mobile ions occurred through kaolinite authigenesis by transformation. This view is consistent with the presence of goethite and gibbsite in unconsolidated sediments of the Botucatu Formation (Fagundes & Zuquette, 2011).

5.3. Clay transformation in the Plata River

The clay composition of the Pantanal back-bulge is distinguishable from the Andean foreland basin clays. The Paraguay, Paraná, and Uruguay Rivers are the primary sources of kaolinite to the Plata River estuary (Table S7), which ranges from 50 – 75% in the suspended load (Figure 13) (Depetris & Griffin, 1968; Manassero et al., 2008). Samples downstream of the Pantanal outlet were commonly 15 – 20% kaolinite, indicating dilution of the kaolinite by sub-Andes-derived illite. The Bermejo River is an example of concentrated illite supply to the Paraguay River (Bertolino & Depetris, 1992; McGlue et al., 2016; Repasch et al., 2021). Bermejo clays were <5% kaolinite near the thrust front, and the kaolinite remained <5% as far as 40 km downstream (Bertolino & Depetris, 1992). Illite comprised ~60% of clay composition throughout the length of the Bermejo River to its confluence with the Paraguay River. Other rivers such as the Pilcomayo and the Salado Rivers that drain the Andean thrust belt were similarly enriched in illite (Bertolino & Depetris, 1992; McGlue et al., 2016). We ascribe the dilution of kaolinite in the Paraguay and Paraná Rivers to these illite-rich clay compositions draining the Andean foothills. The back-bulge and interior craton are dominated by kaolinite, thereby creating ancient wetland deposits that are also rich in kaolinite (e.g., Tineo et al., 2022). In contrast, the thrust front sediments are dominated by illite and smectite, with the latter influenced by the dry climate of the Chaco Seco (McGlue et al., 2016).

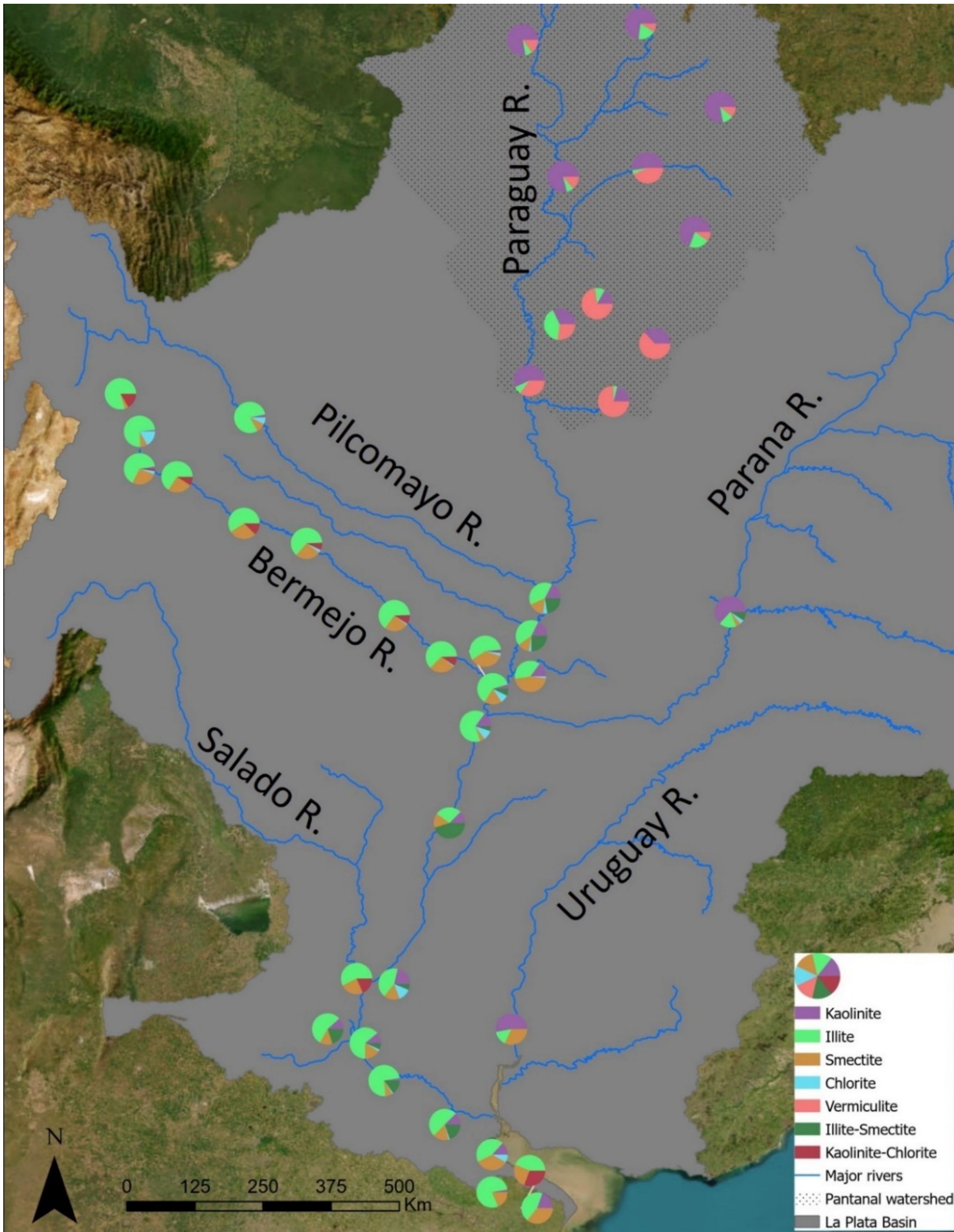

Figure 13: Summary of mud transport from the Paraguay River to the confluence with the Pilcomayo, Bermejo, Paraná, and Salado Rivers to the Plata River mouth. Data (*n = 84*) from past studies (Depetris & Griffin, 1968; Bertolino & Depetris, 1992; Ronco et al., 2001; Manassero et al., 2008; McGlue et al., 2016) (Table S7). Pantanal samples in the hatched area are from this study. The rivers were obtained from the HydroSheds database (Lehner et al., 2008), and the Plata River watershed was downloaded from the Transboundary Freshwater Diplomacy Database, College of Earth, Ocean, and Atmospheric Sciences, Oregon State University. Additional information about the TFDD can be found at: https://transboundarywaters.oregonstate.edu.

We find that the dominantly kaolinite clay composition at the Pantanal outlet is controlled by climate > soil > lithology. We interpret that because vermiculite clays were not present in downstream clay fractions, this observation suggests that vermiculite might be diluted by illite as it exits the Pantanal Basin. In addition to this dilution effect, we identify three potential factors for the rapid change in clay composition. First, the decreased kaolinite in the Paraguay and the Paraná Rivers roughly coincide with the boundary between tropical savanna climate (Aw) and the humid subtropical (Cfa) zones (Beck et al., 2018). Campodonico et al. (2016) demonstrate that the CIA decreases downstream in the higher latitude and sub-tropical climate regions. Second, the adjacent lithologies may be supplying illite locally to the fluvial clays. Illite was formed from burial diagenesis (Lanson et al., 2002) and locally eroded into the Paraguay River as it flowed past the Rio Apa craton, which diluted the sediment samples. The lower Paraguay River flows adjacent to the Carboniferous Coronel Oviedo Group, consisting of shale, arenite, diamictite, and glacial tills (Orué, 1996). Third, kaolinite-rich clays might be preserved near the wetland but not preserved in much farther downstream sediments. Further systematic investigations of downstream clay compositions and heavy mineral suites to constrain the controls on clay composition in the entire Plata River catchment is warranted. This study of modern fluvial clays is an important contribution to understanding clay distribution in modern river sediments and provides a key source of information to improve the accuracy of global clay distribution models (Ito & Wagai, 2017; Warr, 2022).

6. Conclusions

This study of modern fluvial clays plus silt from 74 sampling sites revealed the spatial distribution of clay minerals and major fine-fraction chemical elements across an extant tropical back-bulge basin. Mineralogy and chemical weathering indices (CIA and WIP) showed distinct areas of clay generation among the provenance regions. The controls on fine-fraction mineralogy were systematically assessed, and the implications for the downstream fine sediment in the Plata River were summarized.

- The clay proportions follow the rank order pattern of kaolinite > vermiculite > illite > smectite, but these clays are not evenly distributed. The Taquari River forms a prominent E-W trending hinge across the Pantanal Basin, where more intensive leaching and soil authigenesis produce more kaolinite north of the river. Vermiculite was more common south of the Taquari River, and illite was most common along the North Paraguay Belt. Gibbsite and goethite in the clay-sized fraction signaled contribution from heavily weathered soils such as laterites.

- Major elemental geochemistry of the clay plus silt was used to calculate average CIA = 76.4 and average WIP = 27.6 throughout the Pantanal. The medial Pantanal Basin is highly weathered at the confluence of the Taquari and Paraguay Rivers, representing the cumulative weathering effects of the northern Pantanal. The southern Pantanal fine sediments along the Rio Apa craton and the South Paraguay Belt were poorly weathered, displaying greater values of CaO, Na_2O, and K_2O consistent with climate and parent rocks.

- The main controls on modern fluvial clay plus silt were climate > soil > parent rock. This interpretation was supported by the Taquari River weathering hinge, where kaolinite-rich clays north of the river were linked to greater precipitation and shorter dry season. This same region also contained more kaolinite-rich soils such as acrisols and ferralsols. In contrast, mollisols and luvisols coupled with reduced precipitation and longer dry seasons in the southern Pantanal allowed for more detrital clays: illite and vermiculite. Illite was especially linked to low-grade metamorphic lithologies present only in the Paraguay Belt.

- The Pantanal Basin's clay mineral composition near the basin outlet is primarily kaolinite and vermiculite, contrasting sharply with detrital back-bulge clays from the sub-tropics (Bermejo, Pilcomayo, etc.), which are dominated by illite and smectite. The illite transported from the sub-Andean regions significantly dilutes the proportion of kaolinite in the Plata River. This composition likely generates distinct mudstones in the stratigraphy, with implications for interpretations of the rock record.

7. Acknowledgements

This material is based upon work supported by the National Science Foundation Graduate Research Fellowship Program under Grant No. 1839289. This work was partially supported by a Southern Regional Education Board Doctoral Scholars Program Dissertation Year award, Ferm Fund awards from the Department of Earth and Environmental Sciences at the University of Kentucky, and an NSF/GSA Graduate Student Geoscience Grant #12743-20, which was funded by NSF Award #1949901, to E. Lo. Dr. P. Obura provided XRD guidance, and M. Vandiviere measured sediment pH and graciously provided access to lab equipment and reagents in the making of oriented clay mounts at the University of Kentucky. D.I.S. Dainezi helped process suspended sediment samples at the ecology lab of the *Universidade Federal de Mato Grosso do Sul—Câmpus do Pantanal*. Access to a Katanax fluxer and WD-XRF was made possible by the Kentucky Geological Survey and the expertise of J. Backus and E. Davis. We thank P. Mendez of the *Gobierno Autónomo Departamental de Santa Cruz* for sharing geologic GIS files. Hydrologic data from Bolivia were obtained in person from the *Servicio Nacional de Hidrografía Naval* (SNHN) and the *Servicio Nacional de Meteorología e Hidrología* (SENAMHI). The study received support from the *Conselho Nacional de Desenvolvimento Científico e Tecnológico* (CNPq - Processes: 314986/2020-0 and 431253/2018-8) and a *Bolsa PQ* to A. Silva (Process: 314986/2020-0). The *Fundação de Apoio ao Desenvolvimento do Ensino, Ciência e Tecnologia do Estado de Mato Grosso do Sul* (FUNDECT - Processes: TO 267/2022 and 063/2017) financed fieldwork and research development. This study was supported by the *Fundação Universidade Federal de Mato Grosso do Sul* – UFMS/MEC – Brazil. We are indebted to L. Matchua Souza of the Kadiwéu leadership for access to two sampling sites located in the Kadiwéu indigenous territory. We thank two anonymous reviewers for their thoughtful comments and advice, which have greatly improved this manuscript.

8. Conflict of interest

The authors declare that they have no known competing financial interests or personal relationships that could have appeared to influence the work reported in this paper.

9. Data availability statement

All our relevant datasets are included in supplementary materials.

10. Authors contribution

Conceptualization: E.L.L., M.M.M., and A.S. Logistics and fieldwork: G.G.R., E.L.L., A.S., S.K., and R.O.L. Lab analyses: E.L.L. and K.C.H., with access and training to the soil chemistry lab provided by C.J.M. Writing and figure development: E.L.L., M.M.M., C.J.M., and G.G.R. All authors have read and agreed to the published version of the manuscript.

References

Almeida, F. F. M. de, Hasui, Y., & Neves, B. B. de B. (1976). The Upper Precambrian of South America. *Boletim IG*, *7*, 45–80. https://doi.org/10.11606/issn.2316-8978.v7i0p45-80

Alvarenga, C. J. S., Boggiani, P. C., Babinski, M., Dardenne, M. A., Figueiredo, M. F., Dantas, E. L., Uhlein, A., Santos, R. V., Sial, A. N., & Trompette, R. (2011). Chapter 45 Glacially influenced sedimentation of the Puga Formation, Cuiabá Group and Jacadigo Group, and associated carbonates of the Araras and Corumbá groups, Paraguay Belt, Brazil. *Geological Society, London, Memoirs*, *36*(1), 487–497. https://doi.org/10.1144/M36.45

Ambrosi, J. P., Nahon, D., & Herbillon, A. J. (1986). The epigenetic replacement of kaolinite by hematite in laterite — petrographic evidence and the mechanisms involved. *Geoderma*, *37*(4), 283–294. https://doi.org/10.1016/0016-7061(86)90030-3

Aparicio, P., Ferrell, R. E., & Galán, E. (2010). Mg and K exchange cation effects on the XRD analysis of soil clays. *Philosophical Magazine*, *90*(17–18), 2373–2385. https://doi.org/10.1080/14786430903559417

Aparicio, P., Galán, E., & Ferrell, R. E. (2006). A new kaolinite order index based on XRD profile fitting. *Clay Minerals*, *41*(4), 811–817. https://doi.org/10.1180/0009855064140220

Aristizábal, E., Roser, B., & Yokota, S. (2005). Tropical chemical weathering of hillslope deposits and bedrock source in the Aburrá Valley, northern Colombian Andes. *Engineering Geology*, *81*(4), 389–406. https://doi.org/10.1016/j.enggeo.2005.08.001

Assine, M. L. (2005). River avulsions on the Taquari megafan, Pantanal wetland, Brazil. *Geomorphology*, *70*(3), 357–371. https://doi.org/10.1016/j.geomorph.2005.02.013

Assine, M. L., Merino, E. R., Pupim, F. N., Warren, L. V., Guerreiro, R. L., & McGlue, M. M. (2016). Geology and Geomorphology of the Pantanal Basin. In I. Bergier & M. L. Assine (Eds.), *Dynamics of the Pantanal Wetland in South America* (p. 23–50). Springer International Publishing. https://doi.org/10.1007/698_2015_349

Austin, J. C., Perry, A., Richter, D. D., & Schroeder, P. A. (2018). Modifications of 2:1 Clay Minerals in a Kaolinite-Dominated Ultisol under Changing Land-Use Regimes. *Clays and Clay Minerals*, *66*(1), 61–73. https://doi.org/10.1346/CCMN.2017.064085

Balan, E., Fritsch, E., Allard, T., & Calas, G. (2007). Inheritance vs. neoformation of kaolinite during lateritic soil formation: a case study in the middle Amazon Basin.

Clays and Clay Minerals, *55*(3), 253–259. https://doi.org/10.1346/CCMN.2007.0550303

Barboza, E., Santos, A., Fernandes, C., & Geraldes, M. (2018). Paraguay Belt lithostratigraphic and tectonic characterization: implications in the evolution of the orogen (Mato Grosso-Brazil). *Journal of Sedimentary Environments*, *3*, 54–73. https://doi.org/10.12957/jse.2018.34219

Bauluz, B., Mayayo, M. J., Yuste, A., & López, J. M. G. (2008). Genesis of kaolinite from Albian sedimentary deposits of the Iberian Range (NE Spain): analysis by XRD, SEM and TEM. *Clay Minerals*, *43*(3), 459–475. https://doi.org/10.1180/claymin.2008.043.3.10

Beck, H. E., Zimmermann, N. E., McVicar, T. R., Vergopolan, N., Berg, A., & Wood, E. F. (2018). Present and future Köppen-Geiger climate classification maps at 1-km resolution. *Scientific Data*, *5*(1), 180214. https://doi.org/10.1038/sdata.2018.214

Benedetti, M. M., Curi, N., Sparovek, G., Carvalho Filho, A. de, & Silva, S. H. G. (2011). Updated Brazilian's Georeferenced Soil Database – an Improvement for International Scientific Information Exchanging. In *Principles, Application, and Assessment in Soil Science* (p. 408). https://doi.org/10.5772/29627

Bertolini, G., Marques, J. C., Hartley, A. J., Basei, M. A. S., Frantz, J. C., & Santos, P. R. (2021). Determining sediment provenance history in a Gondwanan erg: Botucatu formation, Northern Paraná Basin, Brazil. *Sedimentary Geology*, *417*, 105883. https://doi.org/10.1016/j.sedgeo.2021.105883

Bertolini, G., Marques, J. C., Hartley, A. J., Da-Rosa, A. A. S., Scherer, C. M. S., Basei, M. A. S., & Frantz, J. C. (2020). Controls on Early Cretaceous desert sediment provenance in south-west Gondwana, Botucatu Formation (Brazil and Uruguay). *Sedimentology, 67(5)*, 2672-2690. https://doi.org/10.1111/sed.12715

Bertolino, S., & Depetris, P. (1992). *Mineralogy of the Clay-Sized Suspended Load from Headwater Tributaries on the Paraná River: Bermejo, Pilcomayo, and Paraguay Rivers* (Vol. 52, p. 19–31).

Bhattacharyya, T., Pal, D. K., & Srivastava, P. (2000). Formation of gibbsite in the presence of 2:1 minerals: an example from Ultisols of northeast India. *Clay Minerals*, *35*(5), 827–840. https://doi.org/10.1180/000985500547269

Biscaye, P. E. (1965). Mineralogy and Sedimentation of Recent Deep-Sea Clay in the Atlantic Ocean and Adjacent Seas and Oceans. *GSA Bulletin*, *76*(7), 803–832. https://doi.org/10.1130/0016-7606(1965)76[803:MASORD]2.0.CO;2

Braga, L. G., Pierosan, R., & Geraldes, M. C. (2019). Paleoproterozoic (2.0 Ga) volcano-plutonism in the southeastern region of the Amazon Craton: Petrological aspects and geotectonic implications. *Geological Journal*, *55*(6), 4352–4374. https://doi.org/10.1002/gj.3686

Brewer, C. J., Hampson, G. J., Whittaker, A. C., Roberts, G. G., & Watkins, S. E. (2020). Comparison of methods to estimate sediment flux in ancient sediment routing systems. *Earth-Science Reviews*, *207*, 103217. https://doi.org/10.1016/j.earscirev.2020.103217

Brown, G., & Brindley, G. W. (1980). X-ray Diffraction Procedures for Clay Mineral Identification. In G. W. Brindley & G. Brown (Eds.), *Crystal Structures of Clay Minerals and their X-Ray Identification* (Vol. 5, p. 305-359). Mineralogical Society of Great Britain and Ireland. https://doi.org/10.1180/mono-5.5

Camargo, M. N., & Bennema, J. (1966). Delineamento esquemático dos solos do Brasil. *Pesquisa Agropecuária Brasileira*, *1*(1), 47–54.

Campodonico, V. A., García, M. G., & Pasquini, A. I. (2016). The geochemical signature of suspended sediments in the Parana River basin: Implications for provenance, weathering and sedimentary recycling. *CATENA*, *143*, 201–214. https://doi.org/10.1016/j.catena.2016.04.008

Caracciolo, L. (2020). Sediment generation and sediment routing systems from a quantitative provenance analysis perspective: Review, application and future development. *Earth-Science Reviews*, *209*, 103226. https://doi.org/10.1016/j.earscirev.2020.103226

Cedraz, V., Julià, J., & Assumpção, M. (2020). Joint Inversion of Receiver Functions and Surface-Wave Dispersion in the Pantanal Wetlands: Implications for Basin Formation. *Journal of Geophysical Research: Solid Earth*, *125*(2), e2019JB018337. https://doi.org/10.1029/2019JB018337

Certini, G., Wilson, M. J., Hillier, S. J., Fraser, A. R., & Delbos, E. (2006). Mineral weathering in trachydacitic-derived soils and saprolites involving formation of embryonic halloysite and gibbsite at Mt. Amiata, Central Italy. *Geoderma*, *133*(3), 173–190. https://doi.org/10.1016/j.geoderma.2005.07.005

Céspedes-Payret, C., Piñeiro, G., Gutiérrez, O., & Panario, D. (2012). Land use change in a temperate grassland soil: Afforestation effects on chemical properties and their ecological and mineralogical implications. *Science of The Total Environment*, *438*, 549–557. https://doi.org/10.1016/j.scitotenv.2012.08.075

Chamley, H. (1989). *Clay Sedimentology*. (p. 623). Springer. https://doi.org/10.1007/978-3-642-85916-8

Chase, C. G., Sussman, A. J., & Coblentz, D. D. (2009). Curved Andes: Geoid, forebulge, and flexure. *Lithosphere*, *1*(6), 358–363. https://doi.org/10.1130/L67.1

Cleaves, E. T., Godfrey, A. E., & Bricker, O. P. (1970). Geochemical Balance of a Small Watershed and Its Geomorphic Implications. *GSA Bulletin*, *81*(10), 3015–3032. https://doi.org/10.1130/0016-7606(1970)81[3015:GBOASW]2.0.CO;2

Cohen, A., McGlue, M., Ellis, G., Zani, H., Swarzenski, P., Assine, M., & Silva, A. (2015). Lake formation, characteristics, and evolution in retroarc deposystems: A synthesis of the modern Andean orogen and its associated basins. *Memoir of the Geological Society of America*, *212*, 309–335. https://doi.org/10.1130/2015.1212(16)

Cole, M. M. (1960). Cerrado, Caatinga and Pantanal: The Distribution and Origin of the Savanna Vegetation of Brazil. *The Geographical Journal*, *126*(2), 168–179. https://doi.org/10.2307/1793957

Coringa, E. de A. O., Couto, E. G., Otero Perez, X. L., & Torrado, P. V. (2012). Atributos de solos hidromórficos no Pantanal Norte Matogrossense. *Acta Amazonica*, *42*, 19–28. https://doi.org/10.1590/S0044-59672012000100003

Corrêa, J. C., Cavallaro, F. A., Garcia, R. H. L., Santos, R. S., Amade, R. A., Bernardes, T. L. da S., Velo, A. F., Mesquita, C. H., & Hamada, M. M. (2021). Chemical and physical analysis of sandstone rock from Botucatu Formation. *Brazilian Journal of Radiation Sciences*, *9*(1A), 1–19. https://doi.org/10.15392/bjrs.v9i1A.1479

Cruz, A. T., Dinis, P. A., Lucic, M., & Gomes, A. (2022). Spatial variations in sediment production and surface transformations in subtropical fluvial basins (Caculuvar River, south-west Angola): Implications for the composition of sedimentary deposits. *The Depositional Record*, *9*(1), 83–98. https://doi.org/10.1002/dep2.208

Deckers, J., Nachtergaele, F., & Spaargaren, O. (2003). Tropical soils in the classification systems of USDA, FAO and WRB. *Evolution of Tropical Soil Science: Past and Future: Workshop Brussels, 6 March 2002*, 79–94.

Deconinck, J. F., Strasser, A., & Debrabant, P. (1988). Formation of illitic minerals at surface temperatures in Purbeckian sediments (Lower Berriasian, Swiss and French Jura). *Clay Minerals*, *23*(1), 91–103. https://doi.org/10.1180/claymin.1988.023.1.09

Delarmelinda, E. A., Souza Júnior, V. S. de, Wadt, P. G. S., Deng, Y., Campos, M. C. C., & Câmara, E. R. G. (2017). Soil-landscape relationship in a chronosequence of the middle Madeira River in southwestern Amazon, Brazil. *CATENA*, *149*, 199–208. https://doi.org/10.1016/j.catena.2016.09.021

Depetris, P. J., & Griffin, J. J. (1968). Suspended Load in the Río De La Plata Drainage Basin. *Sedimentology*, *11*(1–2), 53–60. https://doi.org/10.1111/j.1365-3091.1968.tb00840.x

Depetris, P., & Probst, J.-L. (1998). Variability of the Chemical Index of Alteration (CIA) in the Paraná River Suspended Load. *Mineralogical Magazine*, *62A*. https://doi.org/10.1180/minmag.1998.62A.1.193

Dill, H. G. (2016). Kaolin: Soil, rock and ore: From the mineral to the magmatic, sedimentary and metamorphic environments. *Earth-Science Reviews*, *161*, 16–129. https://doi.org/10.1016/j.earscirev.2016.07.003

dos Santos Vila da Silva, J., Pott, A., & Chaves, J. V. B. (2021). Classification and Mapping of the Vegetation of the Brazilian Pantanal. In G. A. Damasceno-Junior & A. Pott (Eds.), *Flora and Vegetation of the Pantanal Wetland* (p. 11–38). Springer International Publishing. https://doi.org/10.1007/978-3-030-83375-6_2

Drever, J. I. (1973). The preparation of oriented clay mineral specimens for X-ray diffraction analysis by a filter-membrane peel technique. *American Mineralogist*, *58*(5–6), 553–554.

Eberl, D. D., Farmer, V. C., Barrer, R. M., Fowden, L., Barrer, R. M., & Tinker, P. B. (1997). Clay mineral formation and transformation in rocks and soils. *Philosophical Transactions of the Royal Society of London. Series A, Mathematical and Physical Sciences*, *311*(1517), 241–257. https://doi.org/10.1098/rsta.1984.0026

Fagundes, J. R. T., & Zuquette, L. V. (2011). Sorption behavior of the sandy residual unconsolidated materials from the sandstones of the Botucatu Formation, the main aquifer of Brazil. *Environmental Earth Sciences*, *62*(4), 831–845. https://doi.org/10.1007/s12665-010-0570-y

Faleiros, F. M., Pavan, M., Remédio, M. J., Rodrigues, J. B., Almeida, V. V., Caltabeloti, F. P., Pinto, L. G. R., Oliveira, A. A., Pinto de Azevedo, E. J., & Costa, V. S. (2016). Zircon U–Pb ages of rocks from the Rio Apa Cratonic Terrane (Mato Grosso do Sul, Brazil): New insights for its connection with the Amazonian Craton in pre-Gondwana times. *Gondwana Research*, *34*, 187–204. https://doi.org/10.1016/j.gr.2015.02.018

FAO. (1971). *Soil map of the world IV*. UNESCO (p. 193). UNIPUB, Inc.: New York, NY.

Fedo, C. M., Wayne Nesbitt, H., & Young, G. M. (1995). Unraveling the effects of potassium metasomatism in sedimentary rocks and paleosols, with implications for paleoweathering conditions and provenance. *Geology*, *23*(10), 921–924. https://doi.org/10.1130/0091-7613(1995)023<0921:UTEOPM>2.3.CO;2

Fernandes, L. A., & Magalhães Ribeiro, C. M. (2015). Evolution and palaeoenvironment of the Bauru Basin (Upper Cretaceous, Brazil). *Journal of South American Earth Sciences*, *61*, 71–90. https://doi.org/10.1016/j.jsames.2014.11.007

Fick, S. E., & Hijmans, R. J. (2017). WorldClim 2: new 1-km spatial resolution climate surfaces for global land areas. *International Journal of Climatology*, *37*(12), 4302–4315. https://doi.org/10.1002/joc.5086

Fink, J. R., Inda, A. V., Almeida, J. A. de, Bissani, C. A., Giasson, E., & Nascimento, P. C. do. (2014). Chemical and mineralogical changes in a Brazilian Rhodic Paleudult under different land use and managements. *Revista Brasileira de Ciência Do Solo*, *38*, 1304–1314. https://doi.org/10.1590/S0100-06832014000400026

França, A. B., Arajo, L. M., Maynard, J. B., & Potter, P. E. (2003). Secondary porosity formed by deep meteoric leaching: Botucatu eolianite, southern South America. *AAPG Bulletin*, *87*(7), 1073–1082. https://doi.org/10.1306/02260301071

Furian, S., Barbiéro, L., Boulet, R., Curmi, P., Grimaldi, M., & Grimaldi, C. (2002). Distribution and dynamics of gibbsite and kaolinite in an oxisol of Serra do Mar, southeastern Brazil. *Geoderma*, *106*(1), 83–100. https://doi.org/10.1016/S0016-7061(01)00117-3

Furquim, S. A. C., Barbiéro, L., Graham, R. C., de Queiroz Neto, J. P., Ferreira, R. P. D., & Furian, S. (2010). Neoformation of micas in soils surrounding an alkaline-saline lake of Pantanal wetland, Brazil. *Geoderma*, *158*(3), 331–342. https://doi.org/10.1016/j.geoderma.2010.05.015

Garzanti, E., Andó, S., France-Lanord, C., Censi, P., Vignola, P., Galy, V., & Lupker, M. (2011). Mineralogical and chemical variability of fluvial sediments 2. Suspended-load silt (Ganga–Brahmaputra, Bangladesh). *Earth and Planetary Science Letters*, *302*(1), 107–120. https://doi.org/10.1016/j.epsl.2010.11.043

Garzanti, E., Andò, S., France-Lanord, C., Vezzoli, G., Censi, P., Galy, V., & Najman, Y. (2010). Mineralogical and chemical variability of fluvial sediments: 1. Bedload sand

(Ganga–Brahmaputra, Bangladesh). *Earth and Planetary Science Letters*, *299*(3), 368–381. https://doi.org/10.1016/j.epsl.2010.09.017

Garzanti, E., Padoan, M., Setti, M., López-Galindo, A., & Villa, I. M. (2014). Provenance versus weathering control on the composition of tropical river mud (southern Africa). *Chemical Geology*, *366*, 61–74. https://doi.org/10.1016/j.chemgeo.2013.12.016

Garzanti, E., Pastore, G., Resentini, A., Vezzoli, G., Vermeesch, P., Ncube, L., Niekerk, H. J. V., Jouet, G., & Dall'Asta, M. (2021). The Segmented Zambezi Sedimentary System from Source to Sink: 1. Sand Petrology and Heavy Minerals. *The Journal of Geology*, *129*(4), 343–369. https://doi.org/10.1086/715792

Garzanti, E., Resentini, A., Vezzoli, G., Andò, S., Malusà, M., & Padoan, M. (2012). Forward compositional modelling of Alpine orogenic sediments. *Sedimentary Geology*, *280*, 149–164. https://doi.org/10.1016/j.sedgeo.2012.03.012

Garzanti, E., Vermeesch, P., Vezzoli, G., Andò, S., Botti, E., Limonta, M., Dinis, P., Hahn, A., Baudet, D., De Grave, J., & Yaya, N. K. (2019). Congo River sand and the equatorial quartz factory. *Earth-Science Reviews*, *197*, 102918. https://doi.org/10.1016/j.earscirev.2019.102918

Gleyzer, A., Denisyuk, M., Rimmer, A., & Salingar, Y. (2004). A Fast Recursive Gis Algorithm for Computing Strahler Stream Order in Braided and Nonbraided Networks1. *JAWRA Journal of the American Water Resources Association*, *40*(4), 937–946. https://doi.org/10.1111/j.1752-1688.2004.tb01057.x

Goldich, S. S. (1938). A Study in Rock-Weathering. *The Journal of Geology*, *46*(1), 17–58. https://doi.org/10.1086/624619

Guinoiseau, D., Fekiacova, Z., Allard, T., Druhan, J. L., Balan, E., & Bouchez, J. (2021). Tropical Weathering History Recorded in the Silicon Isotopes of Lateritic Weathering Profiles. *Geophysical Research Letters*, *48*(19), e2021GL092957. https://doi.org/10.1029/2021GL092957

Guyot, J. L., Jouanneau, J. M., Soares, L., Boaventura, G. R., Maillet, N., & Lagane, C. (2007). Clay mineral composition of river sediments in the Amazon Basin. *CATENA*, *71*(2), 340–356. https://doi.org/10.1016/j.catena.2007.02.002

Hamilton, S. (2002). Hydrological controls of ecological structure and function in the Pantanal wetland (Brazil). *The Ecohydrology of South American Rivers and Wetlands*, *6*, 133–158.

Han, W., Hong, H. L., Yin, K., Churchman, G. J., Li, Z. H., & Chen, T. (2014). Pedogenic alteration of illite in subtropical China. *Clay Minerals*, *49*(3), 379–390. https://doi.org/10.1180/claymin.2014.049.3.03

Hartley, A. J., Weissmann, G. S., Bhattacharayya, P., Nichols, G. J., Scuderi, L. A., Davidson, S. K., Leleu, S., Chakraborty, T., Ghosh, P., & Mather, A. E. (2013). Soil Development on Modern Distributive Fluvial Systems: Preliminary Observations with Implications for Interpretation of Paleosols in the Rock Record. In S. G. Driese & L. C. Nordt (Eds.), *New Frontiers in Paleopedology and Terrestrial Paleoclimatology: Paleosols and Soil Surface Analog Systems* (Vol. 104, p. 149-

158). SEPM Society for Sedimentary Geology. https://doi.org/10.2110/sepmsp.104.10

Harvey, R. D., & Beck, C. W. (1962). Hydrothermal regularly interstratified chlorite-vermiculite and tobermorite in alteration zones at Goldfield, Nevada. In E. Ingerson (Ed.), *Clays and Clay Minerals* (p. 343–354). Pergamon. https://doi.org/10.1016/B978-1-4831-9842-2.50024-9

Hatzenbühler, D., Caracciolo, L., Weltje, G. J., Piraquive, A., & Regelous, M. (2022). Lithologic, geomorphic, and climatic controls on sand generation from volcanic rocks in the Sierra Nevada de Santa Marta massif (NE Colombia). *Sedimentary Geology*, *429*, 106076. https://doi.org/10.1016/j.sedgeo.2021.106076

He, J., Garzanti, E., Dinis, P., Yang, S., & Wang, H. (2020). Provenance versus weathering control on sediment composition in tropical monsoonal climate (South China) - 1. Geochemistry and clay mineralogy. *Chemical Geology*, *558*, 119860. https://doi.org/10.1016/j.chemgeo.2020.119860

Heiri, O., Lotter, A. F., & Lemcke, G. (2001). Loss on ignition as a method for estimating organic and carbonate content in sediments: reproducibility and comparability of results. *Journal of Paleolimnology*, *25*(1), 101–110. https://doi.org/10.1023/A:1008119611481

Hillier, S. (1995). Erosion, Sedimentation and Sedimentary Origin of Clays. In B. Velde (Ed.), *Origin and Mineralogy of Clays: Clays and the Environment* (p. 162–219). Springer. https://doi.org/10.1007/978-3-662-12648-6_4

Hirata, R., Gesicki, A., Sracek, O., Bertolo, R., Giannini, P. C., & Aravena, R. (2011). Relation between sedimentary framework and hydrogeology in the Guarani Aquifer System in São Paulo state, Brazil. *Journal of South American Earth Sciences*, *31*(4), 444–456. https://doi.org/10.1016/j.jsames.2011.03.006

Holz, M. (2015). Mesozoic paleogeography and paleoclimates – A discussion of the diverse greenhouse and hothouse conditions of an alien world. *Journal of South American Earth Sciences*, *61*, 91–107. https://doi.org/10.1016/j.jsames.2015.01.001

Horbe, A. M. C., Motta, M. B., de Almeida, C. M., Dantas, E. L., & Vieira, L. C. (2013). Provenance of Pliocene and recent sedimentary deposits in western Amazônia, Brazil: Consequences for the paleodrainage of the Solimões-Amazonas River. *Sedimentary Geology*, *296*, 9–20. https://doi.org/10.1016/j.sedgeo.2013.07.007

Horton, B. K. (2022). Unconformity development in retroarc foreland basins: implications for the geodynamics of Andean-type margins. *Journal of the Geological Society*, *179*(3), jgs2020-263. https://doi.org/10.1144/jgs2020-263

Horton, B. K., & DeCelles, P. G. (1997). The modern foreland basin system adjacent to the Central Andes. *Geology*, *25*(10), 895–898. https://doi.org/10.1130/0091-7613(1997)025<0895:TMFBSA>2.3.CO;2

IBGE. (2002). *Mapa de Clima do Brasil*. Instituto Brasileiro de Geografia e Estatística. https://www.ibge.gov.br/geociencias/informacoes-ambientais/climatologia/15817-clima.html

Ito, A., & Wagai, R. (2017). Global distribution of clay-size minerals on land surface for biogeochemical and climatological studies. *Scientific Data*, *4*(1), 170103. https://doi.org/10.1038/sdata.2017.103

Ivory, S. J., McGlue, M. M., Spera, S., Silva, A., & Bergier, I. (2019). Vegetation, rainfall, and pulsing hydrology in the Pantanal, the world's largest tropical wetland. *Environmental Research Letters*, *14*, 124017. https://doi.org/10.1088/1748-9326/ab4ffe

Jackson, M. L. (1969). Soil Chemical Analysis - Advanced Course. *Soil Chemical Analysis - Advanced Course.*, *Edition 2*. (p. 1790)

Johnsson, M. J. (1993). The system controlling the composition of clastic sediments. In M. J. Johnsson & A. Basu (Eds.), *Processes Controlling the Composition of Clastic Sediments* (Vol. 284, p. 1-19). Geological Society of America. https://doi.org/10.1130/SPE284-p1

Johnsson, M. J., & Meade, R. H. (1990). Chemical weathering of fluvial sediments during alluvial storage; the Macuapanim Island point bar, Solimoes River, Brazil. *Journal of Sedimentary Research*, *60*(6), 827–842. https://doi.org/10.1306/212F9296-2B24-11D7-8648000102C1865D

Jonell, T. N., Clift, P. D., Hoang, L. V., Hoang, T., Carter, A., Wittmann, H., Böning, P., Pahnke, K., & Rittenour, T. (2017). Controls on erosion patterns and sediment transport in a monsoonal, tectonically quiescent drainage, Song Gianh, central Vietnam. *Basin Research*, *29*(S1), 659–683. https://doi.org/10.1111/bre.12199

Junk, W. J., da Cunha, C. N., Wantzen, K. M., Petermann, P., Strüssmann, C., Marques, M. I., & Adis, J. (2006). Biodiversity and its conservation in the Pantanal of Mato Grosso, Brazil. *Aquatic Sciences*, *68*(3), 278–309. https://doi.org/10.1007/s00027-006-0851-4

Lacerda Filho, J. V. de, Abreu Filho, W., Valente, C. R., Oliveira, C. C. de, & Albuquerque, M. C. de. (2004). *Geologia e recursos minerais do estado de Mato Grosso*. CPRM; Secretaria de Estado de Indústria, Comércio, Minas e Energia do Estado de Mato Grosso (SICME-MT). http://rigeo.cprm.gov.br/jspui/handle/doc/4871

Lacerda Filho, J. V. de, Brito, R. S. C. de, Silva, M. da G. da, Oliveira, C. C. de, Moreton, L. C., Martins, E. G., Lopes, R. da C., Lima, T. M., Larizzatt, J. H., & Valente, C. R. (2006). *Geologia e recursos minerais do estado de Mato Grosso do Sul*. CPRM; SEPROTUR/MS; EGRHP/MS. http://rigeo.cprm.gov.br/jspui/handle/doc/10217

Lanson, B., Beaufort, D., Berger, G., Bauer, A., Cassagnabère, A., & Meunier, A. (2002). Authigenic kaolin and illitic minerals during burial diagenesis of sandstones: a review. *Clay Minerals 37(1)*: 1-22. https://doi.org/10.1180/0009855023710014

Lehner, B., Verdin, K., & Jarvis, A. (2008). New Global Hydrography Derived From Spaceborne Elevation Data. *Eos, Transactions American Geophysical Union*, *89*(10), 93–94. https://doi.org/10.1029/2008EO100001

Liptzin, D., & Silver, W. L. (2009). Effects of carbon additions on iron reduction and phosphorus availability in a humid tropical forest soil. *Soil Biology and Biochemistry*, *41*(8), 1696–1702. https://doi.org/10.1016/j.soilbio.2009.05.013

Liu, Z., Wang, H., Hantoro, W. S., Sathiamurthy, E., Colin, C., Zhao, Y., & Li, J. (2012). Climatic and tectonic controls on chemical weathering in tropical Southeast Asia (Malay Peninsula, Borneo, and Sumatra). *Chemical Geology*, *291*, 1–12. https://doi.org/10.1016/j.chemgeo.2011.11.015

Lo, E. L., Silva, A., Kuerten, S., Louzada, R. O., Rasbold, G. G., & McGlue, M. M. (2023). Source-to-sink controls on modern fluvial sands in the Pantanal back-bulge basin (Brazil). *Sedimentologika*, *1*(1), 1–18. https://doi.org/10.57035/journals/sdk.2023.e11.1152

Louzada, R. O., Bergier, I., Roque, F. O., McGlue, M. M., Silva, A., & Assine, M. L. (2021). Avulsions drive ecosystem services and economic changes in the Brazilian Pantanal wetlands. *Current Research in Environmental Sustainability*, *3*, 100057. https://doi.org/10.1016/j.crsust.2021.100057

Madeira, J., Bedidi, A., Cervelle, B., Pouget, M., & Flay, N. (1997). Visible spectrometric indices of hematite (Hm) and goethite (Gt) content in lateritic soils: The application of a Thematic Mapper (TM) image for soil-mapping in Brasilia, Brazil. *International Journal of Remote Sensing*, *18*(13), 2835–2852. https://doi.org/10.1080/014311697217369

Manassero, M., Camilión, C., Poiré, D., Da Silva, M., & Ronco, A. (2008). Grain size analysis and clay mineral associations in bottom sediments from Paraná River Basin. *Latin American Journal of Sedimentology and Basin Analysis*, *15*(2), 125–137.

Mathian, M., Bueno, G. T., Balan, E., Fritsch, E., Do Nascimento, N. R., Selo, M., & Allard, T. (2020). Kaolinite dating from Acrisol and Ferralsol: A new key to understanding the landscape evolution in NW Amazonia (Brazil). *Geoderma*, *370*, 114354. https://doi.org/10.1016/j.geoderma.2020.114354

McGlue, M. M., Guerreiro, R. L., Bergier, I., Silva, A., Pupim, F. N., Oberc, V., & Assine, M. L. (2017). Holocene stratigraphic evolution of saline lakes in Nhecolândia, southern Pantanal wetlands (Brazil). *Quaternary Research*, *88*(3), 472–490. https://doi.org/10.1017/qua.2017.57

McGlue, M. M., Silva, A., Assine, M. L., Stevaux, J. C., & Pupim, F. do N. (2015). Paleolimnology in the Pantanal: Using Lake Sediments to Track Quaternary Environmental Change in the World's Largest Tropical Wetland. In I. Bergier & M. L. Assine (Eds.), *Dynamics of the Pantanal Wetland in South America* (p. 51–81). Springer International Publishing. https://doi.org/10.1007/698_2015_350

McGlue, M. M., Smith, P. H., Zani, H., Silva, A., Carrapa, B., Cohen, A. S., & Pepper, M. B. (2016). An integrated sedimentary systems analysis of the Río Bermejo (Argentina): Megafan character in the overfilled Southern Chaco Foreland basin. *Journal of Sedimentary Research*, *86*(12), 1359–1377. https://doi.org/10.2110/jsr.2016.82

Moore, D. M., & Reynolds, R. C. (1989). *X-Ray Diffraction and the Identification and Analysis of Clay Minerals.* (p. 332). Springer.

Nascimento, A. F., Furquim, S. A. C., Graham, R. C., Beirigo, R. M., Oliveira Junior, J. C., Couto, E. G., & Vidal-Torrado, P. (2015). Pedogenesis in a Pleistocene fluvial system of the Northern Pantanal — Brazil. *Geoderma*, *255–256*, 58–72. https://doi.org/10.1016/j.geoderma.2015.04.025

Nesbitt, H. W., & Wilson, R. E. (1992). Recent chemical weathering of basalts. *American Journal of Science*, *292*(10), 740–777. https://doi.org/10.2475/ajs.292.10.740

Nesbitt, H. W., & Young, G. M. (1982). Early Proterozoic climates and plate motions inferred from major element chemistry of lutites. *Nature*, *299*, 715-717. https://doi.org/10.1038/299715a0

Nesbitt, H. W., & Young, G. M. (1984). Prediction of some weathering trends of plutonic and volcanic rocks based on thermodynamic and kinetic considerations. *Geochimica et Cosmochimica Acta*, *48*(7), 1523–1534. https://doi.org/10.1016/0016-7037(84)90408-3

Novello, V. F., Cruz, F. W., Vuille, M., Stríkis, N. M., Edwards, R. L., Cheng, H., Emerick, S., de Paula, M. S., Li, X., Barreto, E. de S., Karmann, I., & Santos, R. V. (2017). A high-resolution history of the South American Monsoon from Last Glacial Maximum to the Holocene. *Scientific Reports*, *7*(1), 44267. https://doi.org/10.1038/srep44267

Ojanuga, A. G. (1973). Weathering of Biotite in Soils of a Humid Tropical Climate. *Soil Science Society of America Journal*, *37*(4), 644–646. https://doi.org/10.2136/sssaj1973.03615995003700040046x

Oliva, P., Viers, J., Dupré, B., Fortuné, J. P., Martin, F., Braun, J. J., Nahon, D., & Robain, H. (1999). The effect of organic matter on chemical weathering: study of a small tropical watershed: nsimi-zoétélé site, cameroon. *Geochimica et Cosmochimica Acta*, *63*(23), 4013–4035. https://doi.org/10.1016/S0016-7037(99)00306-3

Olson, D. M., Dinerstein, E., Wikramanayake, E. D., Burgess, N. D., Powell, G. V. N., Underwood, E. C., D'amico, J. A., Itoua, I., Strand, H. E., Morrison, J. C., Loucks, C. J., Allnutt, T. F., Ricketts, T. H., Kura, Y., Lamoreux, J. F., Wettengel, W. W., Hedao, P., & Kassem, K. R. (2001). Terrestrial Ecoregions of the World: A New Map of Life on Earth: A new global map of terrestrial ecoregions provides an innovative tool for conserving biodiversity. *BioScience*, *51*(11), 933–938. https://doi.org/10.1641/0006-3568(2001)051[0933:TEOTWA]2.0.CO;2

Orué, D. (1996). *Síntese da geologia do Paraguai oriental, com ênfase para o magmatismo alcalino associado* [Thesis, Universidade de São Paulo]. https://doi.org/10.11606/D.44.1996.tde-24092015-163805

Parker, A. (1970). An Index of Weathering for Silicate Rocks. *Geological Magazine*, *107*(6), 501–504. https://doi.org/10.1017/S0016756800058581

Potter, P. E. (1994). Modern sands of South America: composition, provenance and global significance. *Geologische Rundschau*, *83*(1), 212–232. https://doi.org/10.1007/BF00211904

Price, J. R. & Velbel, M. A. (2003). Chemical weathering indices applied to weathering profiles developed on heterogeneous felsic metamorphic parent rocks. *Chemical Geology 202*: 397-416. https://doi.org/10.1016/j.chemgeo.2002.11.001

Quartero, E. M., Leier, A. L., Bentley, L. R., & Glombick, P. (2015). Basin-scale stratigraphic architecture and potential Paleocene distributive fluvial systems of the Cordilleran Foreland Basin, Alberta, Canada. *Sedimentary Geology*, *316*, 26–38. https://doi.org/10.1016/j.sedgeo.2014.11.005

RadamBrasil, P. (1982). Folha SE.21 – Corumbá e parte da Folha SE-20; geologia, geomorfologia, pedologia, vegetação e uso potencial da terra. *Projeto RADAMBRASIL: Levantamento de recursos naturais, 27*. (p. 552). Ministério das Minas e Energia. Secretaria Geral: Rio de Janeiro.

Reatto, A., Bruand, A., de Souza Martins, E., Muller, F., da Silva, E. M., Carvalho, O. A. de, & Brossard, M. (2008). Variation of the kaolinite and gibbsite content at regional and local scale in Latosols of the Brazilian Central Plateau. *Comptes Rendus Geoscience*, *340*(11), 741–748. https://doi.org/10.1016/j.crte.2008.07.006

Repasch, M., Scheingross, J. S., Hovius, N., Lupker, M., Wittmann, H., Haghipour, N., Gröcke, D. R., Orfeo, O., Eglinton, T. I., & Sachse, D. (2021). Fluvial organic carbon cycling regulated by sediment transit time and mineral protection. *Nature Geoscience*, *14*(11), 842–848. https://doi.org/10.1038/s41561-021-00845-7

Repasch, M., Wittmann, H., Scheingross, J. S., Sachse, D., Szupiany, R., Orfeo, O., Fuchs, M., & Hovius, N. (2020). Sediment Transit Time and Floodplain Storage Dynamics in Alluvial Rivers Revealed by Meteoric ^{10}Be. *Journal of Geophysical Research: Earth Surface*, *125*(7), e2019JF005419. https://doi.org/10.1029/2019JF005419

Righi, D., & Meunier, A. (1995). Origin of Clays by Rock Weathering and Soil Formation. In B. Velde (Ed.), *Origin and Mineralogy of Clays: Clays and the Environment* (p. 43–161). Springer. https://doi.org/10.1007/978-3-662-12648-6_3

Rivadeneyra-Vera, C., Bianchi, M., Assumpção, M., Cedraz, V., Julià, J., Rodríguez, M., Sánchez, L., Sánchez, G., Lopez-Murua, L., Fernandez, G., Fugarazzo, R., & Team, T. “3-B.” P. (2019). An Updated Crustal Thickness Map of Central South America Based on Receiver Function Measurements in the Region of the Chaco, Pantanal, and Paraná Basins, Southwestern Brazil. *Journal of Geophysical Research: Solid Earth*, *124*(8), 8491–8505. https://doi.org/10.1029/2018JB016811

Rizzotto, G., & Hartmann, L. (2012). Geological and geochemical evolution of the Trincheira Complex, a Mesoproterozoic ophiolite in the southwestern Amazon craton, Brazil. *Lithos*, *148*, 277–295. https://doi.org/10.1016/j.lithos.2012.05.027

Ronco, A., Camilión, C., & Manassero, M. (2001). Geochemistry of heavy metals in bottom sediments from streams of the western coast of the rio de la plata estuary, Argentina. *Environmental Geochemistry and Health*, *23*(2), 89–103. https://doi.org/10.1023/A:1010956531415

Selvaraj, K., & Chen, C. A. (2006). Moderate Chemical Weathering of Subtropical Taiwan: Constraints from Solid-Phase Geochemistry of Sediments and Sedimentary Rocks. *The Journal of Geology*, *114*(1), 101–116. https://doi.org/10.1086/498102

SERGEOMIN. (2005). *Geologia, Departamento de Santa Cruz (Ae-MAP-0005-B) Escala 1:1,000,000*. Servicio Geológico Técnico de Minas (SERGEOTECMIN), La Paz.

Setti, M., López-Galindo, A., Padoan, M., & Garzanti, E. (2014). Clay mineralogy in southern Africa river muds. *Clay Minerals*, *49*(5), 717–733. https://doi.org/10.1180/claymin.2014.049.5.08

Shover, E. F. (1963). Clay-Mineral Environmental Relationships in Cisco (U. Penn.) Clays and Shales, North Central Texas. *Clays and Clay Minerals*, *12*(1), 431–443. https://doi.org/10.1346/CCMN.1963.0120138

Singer, A. (1980). The paleoclimatic interpretation of clay minerals in soils and weathering profiles. *Earth-Science Reviews*, *15*(4), 303–326. https://doi.org/10.1016/0012-8252(80)90113-0

Souza, E. B. de, Pott, A., Wittmann, F., Parolin, P., Markus-Michalczyk, H., Bueno, M. L., & Damasceno-Junior, G. A. (2021). Composition and Distribution of Woody and Palm Vegetation in the Pantanal Wetland. In G. A. Damasceno-Junior & A. Pott (Eds.), *Flora and Vegetation of the Pantanal Wetland* (p. 443–469). Springer International Publishing. https://doi.org/10.1007/978-3-030-83375-6_9

Souza, E. S. de, Fernandes, A. R., De Souza Braz, A. M., Oliveira, F. J. de, Alleoni, L. R. F., & Campos, M. C. C. (2018). Physical, chemical, and mineralogical attributes of a representative group of soils from the eastern Amazon region in Brazil. *SOIL*, *4*(3), 195–212. https://doi.org/10.5194/soil-4-195-2018

Spinzi, Á. M., & Ramírez, H. M. (2014). *Mapa Geológico del Paraguay, Escala 1:1.000.000*. Viceministerio de Minas y Energía, Asunción.

Stallard, R. F., Koehnken, L., & Johnsson, M. J. (1991). Weathering processes and the composition of inorganic material transported through the orinoco river system, Venezuela and Colombia. *Geoderma*, *51*(1), 133–165. https://doi.org/10.1016/0016-7061(91)90069-6

Taylor, S. R., & McLennan, S. M. (1995). The geochemical evolution of the continental crust. *Reviews of Geophysics*, *33*(2), 241–265. https://doi.org/10.1029/95RG00262

Tineo, D. E., Comerio, M. A., Vigiani, L. H., Kürten Moreno, G. S., & Poiré, D. G. (2022). Tectonic and paleoclimatic controls on the composition of inland wetland deposits, Chaco foreland basin, Central Andes. *Journal of Sedimentary Research*, *92*(2), 112–133. https://doi.org/10.2110/jsr.2021.033

Truckenbrodt, W., Kotschoubey, B., & Schellmann, W. (1991). Composition and origin of the clay cover on North Brazilian laterites. *Geologische Rundschau*, *80*(3), 591–610. https://doi.org/10.1007/BF01803688

USGS. (1996). *Global 30 Arc-Second Elevation (GTOPO30)*. https://doi.org/10.5066/F7DF6PQS

Ussami, N., Shiraiwa, S., & Dominguez, J. M. L. (1999). Basement reactivation in a sub-Andean foreland flexural bulge: The Pantanal wetland, SW Brazil. *Tectonics*, *18*(1), 25–39. https://doi.org/10.1029/1998TC900004

Vanderaveroet, P., Bout-Roumazeilles, V., Fagel, N., Chamley, H., & Deconinck, J. F. (2000). Significance of random illite-vermiculite mixed layers in Pleistocene sediments of the northwestern Atlantic Ocean. *Clay Minerals*, *35*(4), 679–691. https://doi.org/10.1180/000985500547133

Vasconcelos, B. R., Ruiz, A. S., & Matos, J. B. de. (2015). Polyphase deformation and metamorphism of the Cuiabá group in the Poconé region (MT), Paraguay Fold and Thrust Belt: kinematic and tectonic implications. *Brazilian Journal of Geology*, *45*(1), 51–63. https://doi.org/10.1590/23174889201500010004

Velde, B. B., & Meunier, A. (2008). *The Origin of Clay Minerals in Soils and Weathered Rocks* (p. 406). Springer Science & Business Media. https://doi.org/10.1007/978-3-540-75634-7

Verdin, K. L. (2017). Hydrologic Derivatives for Modeling and Analysis—A new global high-resolution database. In *Data Series* (No. 1053) (p. 16). U.S. Geological Survey. https://doi.org/10.3133/ds1053

Viers, J., Dupré, B., Braun, J.-J., Deberdt, S., Angeletti, B., Ngoupayou, J. N., & Michard, A. (2000). Major and trace element abundances, and strontium isotopes in the Nyong basin rivers (Cameroon): constraints on chemical weathering processes and elements transport mechanisms in humid tropical environments. *Chemical Geology*, *169*(1), 211–241. https://doi.org/10.1016/S0009-2541(00)00298-9

Wang, H., Liu, Z., Sathiamurthy, E., Colin, C., Li, J., & Zhao, Y. (2011). Chemical weathering in Malay Peninsula and North Borneo: Clay mineralogy and element geochemistry of river surface sediments. *Science China Earth Sciences*, *54*(2), 272–282. https://doi.org/10.1007/s11430-010-4158-x

Warr, L. N. (2022). Earth's clay mineral inventory and its climate interaction: A quantitative assessment. *Earth-Science Reviews*, *234*, 104198. https://doi.org/10.1016/j.earscirev.2022.104198

Warren, L., Quaglio, F., Simoes, M., Freitas, B., Assine, M., & Riccomini, C. (2015). Underneath the Pantanal Wetland: A Deep-Time History of Gondwana Assembly, Climate Change, and the Dawn of Metazoan Life. In *Handbook of Environmental Chemistry* (p. 1-21). https://doi.org/10.1007/698_2014_326

Weissmann, G. S., Hartley, A. J., Scuderi, L. A., Nichols, G. J., Owen, A., Wright, S., Felicia, A. L., Holland, F., & Anaya, F. M. L. (2015). Fluvial geomorphic elements in modern sedimentary basins and their potential preservation in the rock record: A review. *Geomorphology*, *250*, 187–219. https://doi.org/10.1016/j.geomorph.2015.09.005

Wilson, M. D. (1992). Inherited Grain-Rimming Clays in Sandstones from Eolian and Shelf Environments: Their Origin and Control on Reservoir Properties. In D. W. Houseknecht & E. D. Pittman (Eds.), *Origin, Diagenesis, and Petrophysics of Clay Minerals in Sandstones* (Vol. 47, p. 209-225). SEPM Society for Sedimentary Geology. https://doi.org/10.2110/pec.92.47.0209

Wilson, M. J. (1999). The origin and formation of clay minerals in soils: past, present and future perspectives. *Clay Minerals*, *34*(1), 7–25. https://doi.org/10.1180/000985599545957

Yuan, H., & Bish, D. L. (2010). NEWMOD+, a new version of the NEWMOD program for interpreting X-ray powder diffraction patterns from interstratified clay minerals.

Clays and Clay Minerals, *58*(3), 318–326. https://doi.org/10.1346/CCMN.2010.0580303

Zani, H., Assine, M. L., & McGlue, M. M. (2012). Remote sensing analysis of depositional landforms in alluvial settings: Method development and application to the Taquari megafan, Pantanal (Brazil). *Geomorphology*, *161–162*, 82–92. https://doi.org/10.1016/j.geomorph.2012.04.003